Chapter 17
Mixed-Phase TiO_2 Nanomaterials as Efficient Photocatalysts

Juying Lei, Hong Li, Jinlong Zhang and Masakazu Anpo

Abstract TiO_2, as one of the most promising photocatalysts, exists different phases such as anatase, rutile and brookite. These phases exhibit different properties and consequently different photocatalytic performances. In addition, mixed-phase TiO_2 have been demonstrated to have enhanced photocatalytic activity relative to pure-phase TiO_2. In the past two decades, many research works have been done on the synthesis of different kinds of mixed-phase TiO_2 and their applications to photocatalysis. In this review, we firstly give an introduction of three main types of TiO_2 phases as mentioned above, including their structural properties, stability, phase transformation and photocatalytic activity. And then we pay more attention on the synthesis of the mixed-phase TiO_2. Six preparation methods are introduced in details, which are hydrothermal method, solvothermal method, microemulsion-mediated solvothermal method, sol-gel method, solvent mixing and calcination method and high-temperature calcination method. Following this, three kinds of applications of the mixed-phase TiO_2 in the photocatalysis field are comprehensively highlighted, including photocatalytic production of hydrogen, reduction of CO_2 and degradation of organic pollutants. As the photocatalytic activity of the mixed-phase TiO_2 is usually higher than the single phase TiO_2, the mechanism for the enhancing effects of the mixed phases are discussed. Finally, the existing problems of mixed-phase TiO_2 are summarized and the application prospects of this kind of nanomaterials are outlooked.

H. Li · J. Zhang
Key Lab for Advanced Materials and Institute of Fine Chemicals,
East China University of Science and Technology, 130 Meilong Road,
Shanghai 200237, People's Republic of China
e-mail: jlzhang@ecust.edu.cn

J. Lei
State Environmental Protection Key Laboratory of Environmental Risk Assessment
and Control on Chemical Process, East China University of Science and Technology,
130 Meilong Road, Shanghai 200237, People's Republic of China

M. Anpo (✉)
Department of Applied Chemistry, Graduate School of Engineering,
Osaka Prefecture University, Naka Ku, 1-1 Gakuencho, Sakai 599-8531, Osaka, Japan
e-mail: anpo@chem.osakafu-u.ac.jp

H. Ünlü et al. (eds.), *Low-Dimensional and Nanostructured Materials and Devices*, NanoScience and Technology,
DOI 10.1007/978-3-319-25340-4_17

17.1 Introduction

In recent years, there has been great concern over the many serious environmental problems and lack of natural clean energy resources that we face on a global scale. The increase in world population and industrial growth have all led to accelerated energy consumption and the unabated release of toxic agents and industrial wastes into the air and waterways, leading to pollution-related diseases, global warming and abnormal climatic changes. Thus, environmentally harmonious, clean and safe scientific technologies to address energy as well as pollution and climatic change are major challenges facing most scientists nowadays. Our scientists hope to contribute to the development ecologically clean, safe, and sustainable chemical technologies, materials and processes.

Although there are many approaches to challenge these issues, ever since Honda and Fujishima [1] found the UV light-induced cleavage of water into H_2 and O_2 using a TiO_2 photo-electrode (photosensitizing effect of TiO_2 electrode), there has been enormous interest in the use of TiO_2 and other extended oxide and chalcogenide semiconductors. The purpose is environmental remediation, where organic toxic materials at low concentrations are photocatalytically converted to harmless oxidation products [2–29]. TiO_2 as a photocatalyst has many attractive features; a convenient band gap between its valence band and conduction band of 3.2 eV (ca. 400 nm), high stability, low cost, non-toxicity and good performance in the oxidation of organic pollutants to CO_2 and H_2O. For these reasons, TiO_2-based photocatalysts have received much attention for various applications in the fields of the generation of clean energy and protection of our environment.

As mentioned above, with its various advantages, TiO_2 has attracted many researchers to perform systematic in-depth studies of it, promoting the application process in various areas related to energy and environment. The related research include studies on photocatalytic mechanism [3–5], regulation of crystal structure and morphology [6–15], improvement of photocatalysis and photoelectric conversion efficiency [16–24], expansion of the optical response range [25–29]. However, traditional TiO_2 has defects in the catalytic performance, which are mainly caused by the following two aspects: on one hand, the large band gap limits its adsorption in the UV region ($\lambda \leq 387$ nm), and the absorption of visible light is almost zero, so that the utilization of the sunlight is low efficiency [3–5]; on the other hand, the recombination of photo-generated electrons and holes is facile and serious, which greatly limits the photocatalytic performance of TiO_2 [30, 31].

Researches have demonstrated that, modification of TiO_2 by organic dye photosensitization [32–36], noble metal deposition [37–41] or doping [42–45] and semiconductor compounding [45–49] can effectively improve the photon utilization and reduce the recombination rate of photo-generated electrons with holes, thereby improving its photocatalytic efficiency. However, the above methods have disadvantages such as poor reaction stability and controllability, high cost, complicated operation process amongst others. In these respects, mixed-phase TiO_2 with relatively simple preparation process, low cost and adjustable crystal type has

attracted much attention. In the mixed-phase photocatalyst, the photo-generated electrons and holes can effectively separate in the two-phase interface, thus reducing their recombination rate. Moreover, the rutile in the mixed phases have a narrower band gap, which can enhance the utilization of visible light to some extent. These advantages can improve the comprehensive properties of TiO_2 photocatalyst. Research results have shown that, adding rutile TiO_2 into pure anatase TiO_2 to form mixed-phase TiO_2 of rutile and anatase, can significantly improve the photocatalytic activity of TiO_2 [50–53]. After these studies, other kinds of mixed-phase TiO_2 have also been studied in depth, such as anatase/brookite [54, 55], anatase/brookite/rutile [56] and brookite/TiO_2(B) [57]. The photocatalytic experimental results of these studies showed that, the photocatalytic activity of mixed-phase TiO_2 is higher than that of single-phase TiO_2. This is because different phases of TiO_2 have different band positions; their combination can effectively promote the separation of photo-generated electron-hole pairs. In addition, catalytic "hot spots" are supposed to be created at the interface of different phases, therefore photocatalysis efficiency can be improved [51, 56].

In this review, first, we would like to briefly introduce three main kinds of TiO_2 phases, and then we will focus on recent advances in the development of mixed-phase TiO_2 photocatalysts, including the synthetic methods for the mixed-phase catalysts, the applications of the catalysts to various photocatalytic reaction systems such as photocatalytic hydrogen production, photoreduction of CO_2 and photocatalytic degradation of organic pollutants. Following this the mechanism of enhanced photocatalytic activity of the mixed-phase TiO_2 will be presented. Finally, we will summarize the existing problems and overview the application prospects of the mixed-phase TiO_2.

17.2 Phases of TiO_2

TiO_2 has eight types of crystal phases, which are rutile, anatase, brookite, TiO_2-B, TiO_2-R, TiO_2-H, TiO_2-II, and TiO_2-III [58]. Among them, rutile, anatase and brookite are naturally occurring oxides of titanium at atmospheric pressure and have been researched mostly for applications [59, 60]. The other five phases have also been investigated [61–64], however, because they are high-pressure phases, they are of minor significance for research and development applications. Therefore, we focus on only the phases of rutile, anatase and brookite in this review.

17.2.1 Structure Properties of Rutile, Anatase and Brookite

The three kinds of TiO_2 phases have different crystallographic properties, which are summarized in Table 17.1 [65].

Table 17.1 Crystallographic property of anatase, rutile, and brookite TiO_2

Crystal structure	Density (g/cm^3)	System	Space group	Cell parameters (nm)		
				a	b	c
Rutile	4.240	Tetragonal	D_{4b}^{14}-$P4_2/mnm$	0.4584	–	0.2953
Anatase	3.830	Tetragonal	D_{4a}^{19}-$I4_1/amd$	0.3758	–	0.9514
Brookite	4.170	Rhombohedral	D_{2h}^{15}-Pbca	0.9166	0.5436	0.5135

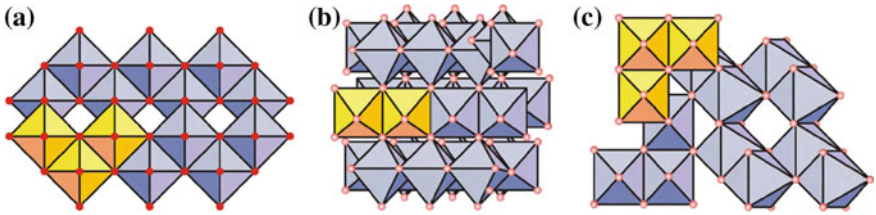

Fig. 17.1 Crystalline structure of **a** anatase, **b** brookite and **c** rutile [68]

In their structures, the basic building block consists of a titanium atom surrounded by six oxygen atoms forming a TiO_6 octahedron in a more or less distorted configuration. In all the three TiO_2 phase structures, the stacking of the TiO_6 octahedra results in threefold coordinated oxygen atoms. The fundamental structural units in these three TiO_2 crystals form from TiO_6 octahedron units and have different lattice configurations as presented in Fig. 17.1. In rutile, TiO_6 octahedra were linked by sharing an edge along the c-axis to form chains. These chains are then interlinked by sharing corner oxygen atoms to form a three-dimensional lattice. Conversely in anatase, the three-dimensional lattice is formed only by edge shared bonding among TiO_6 octahedra. It means that the octahedra in anatase share four edges and are arranged in zigzag chains. In brookite, the octahedra share both edges and corners, forming an orthorhombic structure [66, 67].

In determining these crystal structures and estimating the crystal grain size of anatase, rutile and brookite, the X-ray diffraction (XRD) experimental method is usually used. Anatase peaks in X-ray diffraction occur at $\theta = 12.65°$, 18.9°, and 24.054°, the rutile peaks are found at $\theta = 13.75°$, 18.1°, and 27.2° while brookite peaks are encountered at $\theta = 12.65°$, 12.85°, 15.4°, and 18.1°; θ represents the X-ray diffraction angle [69, 70].

17.2.2 Stability and Phase Transformation

Among the three types of phases, rutile is the most stable phase, which won't decompose or undergo a phase transformation even at very high temperatures. However, anatase and brookite are metastable; they can be transformed into

thermodynamically stable rutile when calcined to a certain temperature. There has been extensive research into the phase transfer mechanism of TiO_2 during heating. Shannon [71] described the anatase to rutile transformation from crystallography to be a nucleation and growth process, in which rutile phase firstly nucleates on the surface of anatase and then expands to the bulk. Due to the great differences between anatase and rutile, the transformation is reconstructive, which means that the transformation process involves the breaking and reforming of bonds [72]. In the course of the transformation to rutile, the {112} planes in anatase are retained as the {100} planes in the rutile product. In these planes, Ti and O atoms synergistically rearrange. Most of the Ti atoms move to a new location to form rutile by the breaking of two Ti-O bonds in the TiO_6 octahedron. Therefore, the formation of oxygen vacancies can accelerate the phase transformation and the formation of Ti interstitials inhibits the transformation. This anatase to rutile transformation is a non-equilibrium phase transformation, which occurs in a certain range of temperature (400–1000 °C); thus temperature is closely related to impurities, particle size, surface area etc. Impurities and processing atmosphere strongly influence the phase transition temperature and rate because they can result in different defect structure. In general, impurities such as the oxides of Ce, Li, K, Na, Fe, and Mn which can increase the oxygen vacancies usually promote the phase transformation, while impurities like S, P, and W usually inhibit the phase transformation. A reductive atmosphere such as H_2 and Cl_2 accelerate the transformation and gases which are conducive to the formation of Ti interstitials slow the phase transformation.

Artificial preparation favors the synthesis of anatase nanoparticles, especially the preparation of TiO_2 in aqueous solution [73]; this is because the energy of the three types of phases are quite close. When the nanoparticles are small enough (<13 nm), the small surface free energy will become the determinant for the phase transformation [74]. For TiO_2 nanocrystals smaller than 11 nm, anatase is the most stable phase. When the nanocrystals are bigger than 35 nm, the rutile phase reflects the thermodynamic stability. And the stability of brookite lies between the anatase and rutile. In fact, brookite as a metastable phase, most of its physical parameters are between those of anatase and rutile, such as the band width of anatase, brookite and rutile are 3.19, 3.11 and 3.0 eV respectively [75].

17.2.3 Photocatalytic Activity of Rutile, Anatase and Brookite

Generally, anatase exhibits the highest photocatalytic activity among the three types of phases, which are due to the following reasons:

(1) The band gap of rutile, anatase and brookite are 3.19, 3.11 and 3.0 eV respectively [75], from which we can see that anatase has the widest band gap. Therefore, the electron-hole pair has more positive or more negative potential, leading to higher oxidation ability [76];

(2) The surface of anatase has a strong adsorption ability for H_2O, O_2 and OH, which is favorable for high photocatalytic activity because the adsorption capacity of the surface has a great influence on the catalytic activity in the photocatalytic reaction and strong adsorption capacity is beneficial to high activity;
(3) Compared to rutile and brookite, anatase usually has smaller grain size and larger specific surface area in the process of crystallization, which can improve the photocatalytic activity.

However, because the photocatalytic activity is also greatly influenced by the crystallization process, the above rules are not suitable for all situations. Under the same conditions, when the amorphous TiO_2 crystallize, rutile usually forms large grains with poor adsorption ability and thus has low catalytic activity. But if the rutile can have the same grain size and surface properties as anatase, it can also have high photocatalytic activity. For example, Lee et al. [77] found that anatase TiO_2 can transfer to rutile TiO_2 by laser exposure. During the transformation, the specific surface area and grain size remained unchanged. This resultant rutile photocatalyst exhibited considerable high catalytic activity. Tsai et al. [78] prepared anatase and rutile TiO_2 by different methods and investigated their photocatalytic activity toward degradation of phenol. They found the catalytic activity was related to the preparation methods and calcinations temperature. Under certain conditions, rutile TiO_2 exhibited very high catalytic activity. Therefore, whether anatase or rutile, they are both likely to have high photocatalytic activity which greatly depends on the surface properties and the grain size. In addition, Ohno et al. [79] reported that the photocatalytic activity of different phases of TiO_2 is related to the electron acceptors in the system. When the electron acceptor is O_2, the photocatalytic activity of anatase is high while that of rutile is relatively low. And when Fe^{3+} is the electron acceptor, rutile showed higher catalytic activity. This is because O_2 as an electron acceptor is quite sensitive to properties of the catalyst materials in the photocatalytic reactions. The surface structure of rutile and/or its low energy band may make it have low transfer efficiency of electrons to O_2 and thus rutile has low catalytic activity when O_2 is the electron acceptor. And because most researchers use O_2 for the studies of photocatalytic reactions, rutile usually exhibits low catalytic activity.

The photocatlytic activity of brookite is quite controversial; the main reasons may be that there have been few studies and experiments on brookite and it is difficult to prepare pure brookite TiO_2. The general products are mixed-phase TiO_2, including anatase/brookite [80], brookite/rutile [81] or anatase/brookite/rutile [44].

Recent studies have demonstrated that, the mixed phase composited TiO_2 crystals in an appropriate composition ratio have higher photocatalytic activity than that of single phase TiO_2 crystal. Bacsa et al. [82] found that 100 % anatase or 100 % rutile has relatively lower photocatalytic activity, but a mixture of anatase and rutile in various ratios achieved better catalytic activity than pure anatase or pure rutile; the mixture with 30 % rutile and 70 % anatase showed the best catalytic activity. Thus the two kinds of crystals have a certain synergistic effect for

enhanced photocatalysis. And the commercial photocatlyst P25, which has considerable high photocatalytic activity, is also a kind of mix-phase TiO_2 rather than pure anatase. Therefore, great efforts have been devoted to investigating the synthesis and photocatalysis applications of mixed-phase TiO_2.

17.3 Synthesis of Mixed-Phase TiO_2 Photocatalysts

It can be observed from the structure and properties of the three types of crystals, that adjusting the experimental parameters of the synthesis can cause conversion among different phase types allowing different mixed-phase TiO_2 photocatalysts to be prepared. At present, there is a variety of methods to prepare mixed-phase TiO_2, such as pulsed laser deposition (PLD), hydrolysis method, hydrothermal method, solvothermal method, micromulsion-mediated solvothermal method, solvent mixing and calcination method (SMC method), high-temperature calcination method, and high temperature gas phase decomposition method as well as others [83]. In the preparation process of mixed-phase TiO_2, with different synthesis methods, the important influence factors for the ratio of mixed phase crystals are different. In all kinds of synthesis methods, the mixed phase ratio, morphology and surface properties can be controlled by optimizing the experimental conditions, such as temperature, pressure, concentration, and types of reagents. The ratio of different crystals in a perfect mixed-phase photocatalyst should be able to be tuned according to the actual needs, and the product should have controllable shape, uniform dispersion, and should be uneasy to agglomerate. The preparation conditions and influence factors will be discussed in the following sub-section, combining concrete preparation methods.

17.3.1 Hydrothermal Method and Solvothermal Method

The hydrothermal method is used most commonly in the laboratory preparation of TiO_2 nanomaterials [84–91]. It refers to a method of synthesizing materials in a sealed reaction vessel (such as an autoclave), using aqueous solution as the reaction system, by heating or other means, to create an environment of high temperature and high pressure. In this condition, the vapor pressure of water becomes higher while the density and surface tension decrease and the ion product increases. This leads to dissolution and recrystallization of the substances which are insoluble in water at room temperature. This method belongs to the liquid phase chemical synthesis method. The main factors influencing the properties of the product by the hydrothermal method include vessel volume, reaction temperature, reaction time, and heating rate.

Chen and Sum et al. [92] synthesized highly crystalline pure brookite and two-phase anatase/brookite TiO_2 nanostructures via a simple hydrothermal method with TiS_2 as the precursors in NaOH solutions. The control of the phase composition has been achieved by varying the solution concentration and reaction time. In the reaction system, the TiS_2 underwent a hydrolysis reaction as follows:

$$TiS_2 + 4\,NaOH \rightarrow Ti^{4+} + 4\,OH^- + 2\,Na_2S \tag{17.1}$$

$$Ti^{4+} + x(OH)^- \rightarrow Ti(OH)_x^{4-x} \tag{17.2}$$

At the beginning of the reaction, the hydrolysis of TiS_2 formed Ti^{4+} (17.1). Then in the hydrothermal process, Ti^{4+} reacted with OH^- in the solution (17.2). When the concentration of OH^- is low, the hydrolysis rate of Ti^{4+} is slow and the Ti^{4+} connect with OH^- to form anatase TiO_2; when the OH^- concentration is high, the hydrothesis rate of Ti^{4+} is fast leading to the formation of mixed-phase TiO_2 of brookite and anatase. The mass fraction of brookite (B) and anatase (A) can be obtained respectively by calculating with the following formula [93]:

$$W_B = K_B I_B / (K_A I_A + K_B I_B) \tag{17.3}$$

$$W_A = K_A I_A / (K_A I_A + K_B I_B) \tag{17.4}$$

In the formula, I_A and I_B represent the integral intensity of the strongest diffraction peaks in anatase and brookite respectively, and $K_A = 0.886$, $K_B = 2.721$. Figure 17.2a, b show the influences of different NaOH concentrations and different reaction times on TiO_2 crystal. From the graphs, it is observed that with increase of NaOH concentration, the content of brookite increases, and when the reaction time is more than 6 h, the crystalline form of the product did not change significantly. In addition, brookite can be obtained by conversion of sodium titanate. Since Na^+ is able to stabilize the layered structure, when there is no Na^+ in the reaction system, a layered structure is not stable, and the hydrothermal process causes the structure to collapse, forming anatase TiO_2; when Na^+ is excessive, the layered structure is very stable and does not easily collapse, ultimately forming titanate; when Na^+ is moderate, the layered structure partially collapses, and part of the layered structure remains unstable, forming brookite (Fig. 17.2c). The above results are consistent with the literature [88].

Zhang et al. [94] introduced NaCl and NH_4OH in the same time into the hydrothermal reaction system, using $TiCl_3$ as a titanium source. The results showed that the phase composition of the products can be controlled by changing the concentration of NaCl and the volume ratio of NH_4OH to H_2O in the reaction system (Fig. 17.3a). They also believe that Na^+ is able to stabilize the layered titanate structure, which was formed by the hydrolysis of $TiCl_3$ in aqueous ammonia in their reaction system. In the absence of NaCl, NH_4^+ ions exist in the interlayer of titanate to balance the negative charges of the layered titanate. However, under hydrothermal treatment at high temperature up to 200 °C, NH_4^+ is

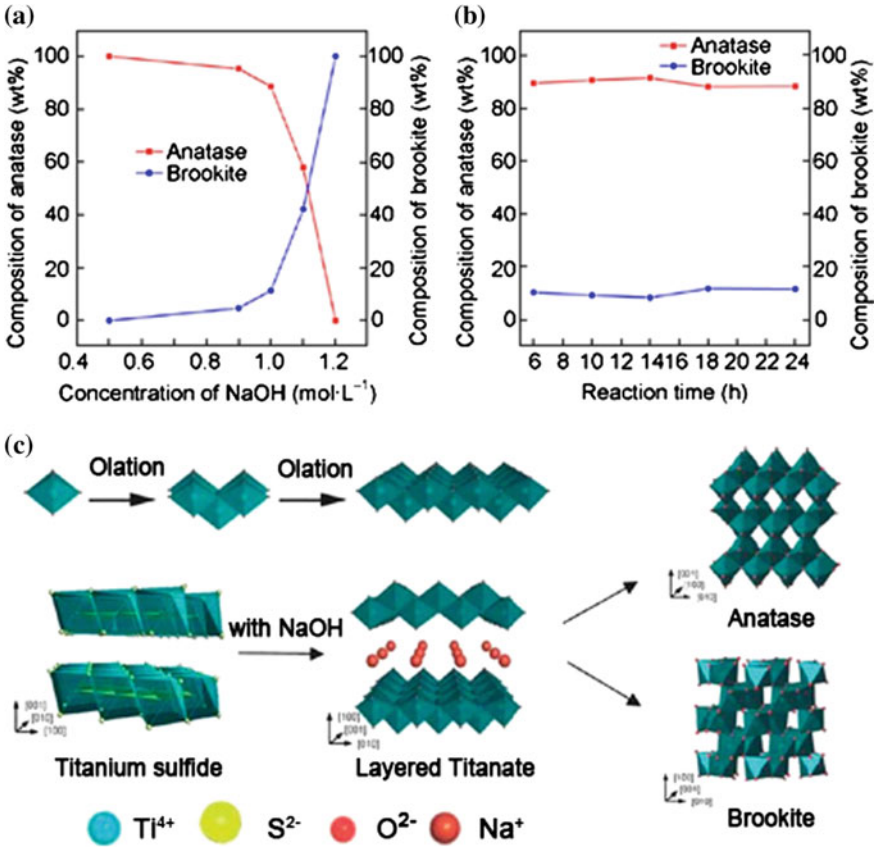

Fig. 17.2 The composition of anatase and brookite in the mixed phase TiO_2 synthesized with **a** various NaOH concentrations and **b** reaction times under hydrothermal reaction [92]; The scheme of formation of anatase and brookite (**c**) [92]

hydrolyzed to form NH_4OH and is released from the interlayer. The H^+ ions produced from the hydrolysis of NH^{4+} ions then induce a hydroxyl condensation reaction to form anatase TiO_2. In the presence of NaCl, Na^+ can help to stabilize the layered structure with NH_4^+. Na^+ and NH_4^+ exist simultaneously in the interlayer of titanate to balance the negative charges of titanate. When the layered titanate was treated hydrothermally continuously at a high temperature for several hours, the increased hydrolysis of NH_4^+ led to the collapse of layered structures. However, some bonds in the structure are maintained by Na^+ ions. Therefore, the structural transformation is delayed which results in the formation of a brookite-like structure [95–97]. The as-formed brookite-like structure expands to form a brookite lattice. Increasing the concentration of NaCl will enhance the powder of the brookite lattice to compete with the anatase lattice. Therefore, the brookite content in the mixed-phase TiO_2 increases with an increase in concentration of NaCl. In addition

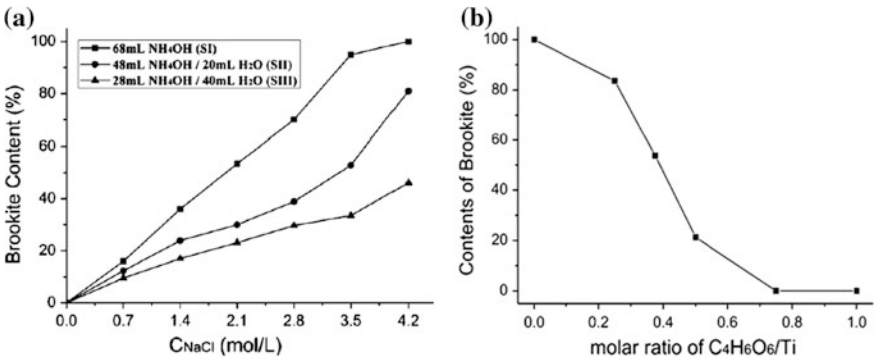

Fig. 17.3 **a** Relationship between the contents of brookite in products and the applied concentration of NaCl [94]; **b** Relationship between the contents of brookite and the applied molar ratio of tartaric acid to $TiCl_3$ [98]

to this research, Zhang et al. [98] developed another facial hydrothermal method for the preparation of anatase/brookite TiO_2 using tartaric acid ($C_4H_6O_6$) as the phase content regulator. Different amounts of $C_4H_6O_6$ were added to the hydrothermal reaction system using $TiCl_3$ as the titanium source and NaOH for adjusting the pH of the reaction solution. The contents of anatase and brookite in the TiO_2 particles were successfully controlled by simply adjusting the molar ratio of $C_4H_6O_6$ to $TiCl_3$ (Fig. 17.3b). The mechanism of the phase evolution between brookite and anatase was explained according to the ligand field theory [99]. They suggested that $C_4H_6O_6$ can chelate with Ti to form a stable titanium complex. When the $C_4H_6O_6$/$TiCl_3$ molar ratio is less than 0.75 in the reaction system, there are two forms of Ti species. One is the insoluble Ti-contained species $Ti(OH)_4$; the other is the soluble Ti-contained complex [Ti(OH)x($C_4H_6O_6$)y]z-. The amorphous $Ti(OH)_4$ could first transform to layered titanate under hydrothermal treatment, which would be transformed to brookite under a given concentration of Na^+ and OH^- [95]. Due to the large steric hindrance of carboxylic acidic ligands, the [Ti(OH)x($C_4H_6O_6$)y]z- complexes should combine together by sharing equatorial or apical edges and being arranged in zigzag chains, which benefited the formation of anatase crystallites, thus resulting in an anatase/brookite mixed-phase TiO_2. They also pointed out that the brookite as the pure phase or the main phase was not obtained when the pH value of the system was less than 9 or the hydrothermal temperature was lower than 180 °C. That is to say, it is difficult to control the contents of anatase and brookite in samples by changing the $C_4H_6O_6$/$TiCl_3$ molar ratio while pH < 9 or temperature <180 °C in the hydrothermal reaction system.

A variation of the hydrothermal method is the solvothermal method wherein organic solvents such as ethanol, glycol and toluene are used instead of an aqueous environment. Similar to the hydrothermal method, in the solvothermal method the crystal types and morphology of the TiO_2 nanomaterials can both be controlled by

regulating parameters such as temperature, pressure inside the system, the reaction time, and the titanium source.

Li et al. [100] synthesized anatase/rutile mixed-phase TiO_2 with different rutile content using the solvothermal method. They obtained mixed-phase TiO_2 crystals by hydrolysis of tetraisopropyltitanate in an acid alcoholic solution and studied the effect of hydrochloric acid on the rutile content in the mixed-phase crystal. The results showed that low H_2O/Ti mole ratio favors the formation of anatase/rutile mixed-phase TiO_2, otherwise it will form brookite/anatase mixed-phase TiO_2. Lei et al. [101] prepared anatase/rutile mixed-phase TiO_2 crystal in a low temperature (80 °C) solvothermal reaction by pre-oxidizing $TiCl_3$ into Ti^{4+} with HNO_3 followed by diluting with urea, water and ethanol. The anatase content in the mixed-phase crystal increases with the increase of ethanol content in the solution (Fig. 17.4). The Scherrer formula is used to calculate the average particle size of anatase and rutile in the mixed-phase crystal; they were both below 10 nm.

The mixed-phase TiO_2 nanomaterials prepared by hydrothermal and solvothermal methods are usually well crystallized and don't need to be calcinated under high temperature. The size and phase type of the product can be regulated by simply changing the experimental parameters such as the type of acid or base in the reaction system, the reaction temperature, the reaction time, the autoclave pressure and so on. Besides these advantages, they also have some drawbacks including the requirement for the equipment to withstand high temperature and high pressure, and experimental safety concerns. Moreover, because the hydrothermal and solvothermal process can't be monitored in real time and usually proceeds without stirring, sometimes the reaction is incomplete and it is difficult to obtain uniform product. Since a variety of organic solvents can be used in the solvothermal method, it is easier to control the morphology and crystalline of the products compared with the hydrothermal method. Thus, the solvothermal method is considered to have better application prospects.

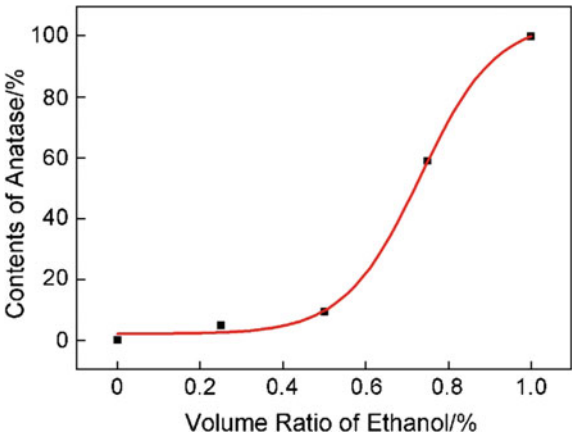

Fig. 17.4 Relationship between the contents of anatase and the volume ratio of ethanol in a solvothermal reaction [101]

17.3.2 Microemulsion-mediated Solvothermal Method

The method of microemulsion refers to the process that, firstly, two immiscible solvents form emulsion in the role of surfactants, and then nanomaterials are obtained in the emulsion through nucleation, coalescence, agglomeration, and heat treatment in the oil-in-water or water-in-oil micro-bubbles. In this process, the two immiscible solvents are divided into many micro-reactors (micro-bubbles) by surfactant, in which the reactants are well dispersed and a uniform nucleation occurs. In addition, the growth of the nucleus can be limited in the micro-reactors. Therefore, the particle size and stability of the nanomaterials can be controlled precisely. Compared with other traditional preparation methods, the microemulsion method has been found to have obvious advantages in terms of the synthesis of nanomaterials with superior monodispersity and interfacial properties. Moreover, this method is a very versatile technique which allows the preparation of a great variety of nanomaterials in combination with other techniques. Recently, the combination of the microemulsion method with solvothermal method, namely the microemulsion-mediated solvothermal method, has been used to prepare the mixed-phase TiO_2 crystals [66, 102, 103].

Yan et al. [66] prepared anatase/rutile mixed-phase TiO_2 crystal through the combination of microemulsion and solvothermal method. In the reaction system, tert-octylphenoxypolyethoxyethanol (Triton X-100) as the surfactant and n-hexanol as the co-surfactant were mixed with cyclohexane to serve as the continuous oil phase. Tetrabutyl titanate and $(NH_4)_2SO_4$ were dissolved in the hydrochloric acid as the aqueous phase. The aqueous phase was added dropwise to the oil phase, forming a clear microemulsion, which was then solvothermally treated below 120 °C for 13 h giving the mixed-phase TiO_2 product. The resultant product has surface area of about 86–169 m^2/g and grain sizes of anatase and rutile of about 15 nm and 10 nm respectively. Their results showed that the change of SO_4^{2-} concentration impacts the content of anatase in the mixed-phase crystal (Fig. 17.5). With the increase of SO_4^{2-} concentration, the anatase content in the mixed-phase TiO_2 crystal increased. Different polymorphs can be obtained by affecting the polycondensation of TiO_6 octahedra with SO_4^{2-} (Fig. 17.6a). The SO_4^{2-} interacts with the hydroxy groups on the surface of TiO_6 octahedra to form hydrogen bonds during the hydrothermal reaction process (Fig. 17.6b). Because of the steric effect of SO_4^{2-}, the octahedron with SO_4^{2-} and another octahedron would polycondense along the converse direction in order to decrease the repulsion (Fig. 17.6c), and the orientation of the third octahedron is more conducive to the formation of an anatase nucleus (Fig. 17.6d). When the concentration of SO_4^{2-} stays at a lower level, a rutile structure can be easily formed in order to ensure the lowest free energy in the system. Therefore, controlled adjustment of anatase content in mixed TiO_2 crystal can be achieved by adjusting the concentration of SO_4^{2-}. In the same oil phase system, Zhang et al. [103] prepared mixed-phase TiO_2 crystal with different anatase and rutile content by the microemulsion-mediated solvothermal method, using a mixture of $TiCl_3$, urea, and hydrochloric acid solution as the aqueous phase. The results

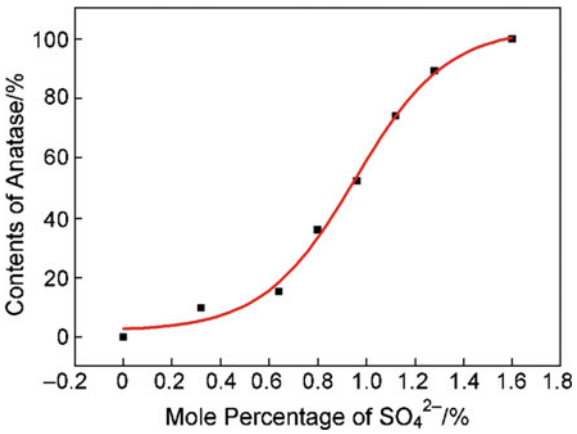

Fig. 17.5 Relationship between the contents of anatase and the mole percentage of SO_4^{2-} under the micromulsion-mediated hydrothermal method [66]

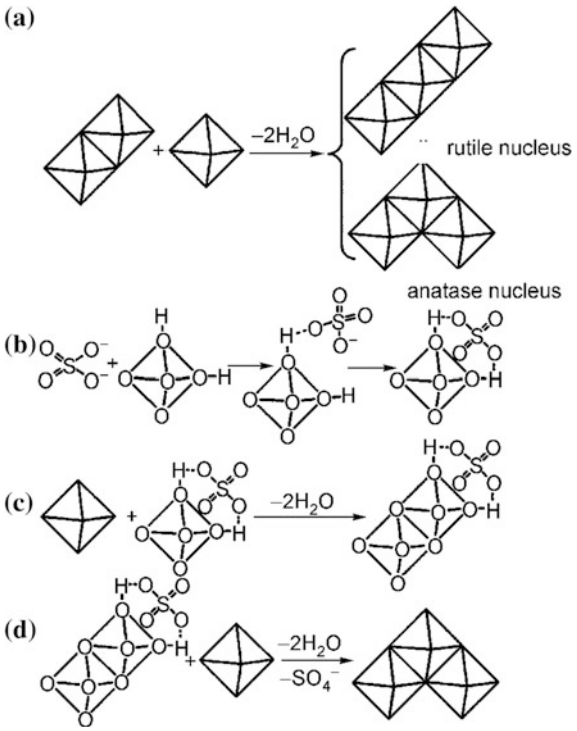

Fig. 17.6 Proposed mechanism: **a** the orientation of the third octahedron determines whether a rutile or an anatase nucleus is formed; **b** interaction between SO_4^{2-} and TiO_6^{2-} octahedral hydroxyls; **c** two TiO_6^{2-} octahedra share edge in the presence of SO_4^{2-}; **d** formation of anatase in the presence of SO_4^{2-} [66]

showed that with the increase of urea concentration, anatase content in the mixed-phase TiO_2 increased. The hydrochloric acid in the reaction solution suppressed the generation of anatase and promoted the formation of rutile phase. Different from SO_4^{2-}, the Cl^- has small radius and weak steric hindrance. TiO_6 octahedra polycondensed in chain to form a rutile structure according to the

minimum energy principle. Therefore, high concentration of Cl^- favors the formation of rutile TiO_2 and a high concentration of SO_4^{2-} favors the formation of anatase TiO_2.

Although the experiment process is relatively complicated in the preparation of mixed-phase TiO_2 by the microemulsion-mediated solvothermal method, the grain size of the product is small and the phases can be controlled, which gives this method good prospects for development.

17.3.3 Sol-Gel Method

Sol-gel method is one of the commonly used methods for preparation of TiO_2 nanomaterials. The sol-gel method has advantages such as processing at low-temperature and the ability to prepare materials in various shapes, thus, it is one of the most promising techniques to prepare amorphous and crystalline materials. Usually the titanium precursor used in the sol-gel reaction system is titanium alkoxides or titanium halides. Firstly, a sol is prepared by hydrolysis of titanium precursor. After aging the sol for a certain time, a three-dimensional cross-linked gel is obtained; amorphous white powder is obtained after grinding the gel. Finally, crystallized TiO_2 is produced by high temperature calcination.

Scotti et al. [52] synthesized anatase/rutile mixed-phase TiO_2 crystal by a sol-gel method and investigated the influence of HCl/Ti and H_2O/Ti molar ratio on the phase type of the product. The experimental process was as follows: $TiCl_4$ and tri-block copolymer were dissolved in ethanol then water and HCl were added to adjust the pH of the solution, obtaining a sol. A gel is formed after aging the sol for 3–13 days. After drying and calcination, TiO_2 crystals with different anatase and rutile content were obtained. In the products, pure rutile phase (Fig. 17.7a) showed chestnut burr aggregates of radially growing elongated nanocrystals with average sizes of 10–20 nm in width and 100–200 nm in length; pure anatase phase (Fig. 17.7b) showed aggregates of almost square-ended nanoparticles with average sizes of 5–15 nm. The mixed-phase sample (Fig. 17.7c) was observed to have two phases with the small anatase particles surrounding the chestnut burr aggregates of rutile. The phase content of the products can be controlled by systematically changing the H_2O:Ti (rw) and HCl:Ti (ra) molar ratios in the reaction system. Results have shown that, in the acidic titanium halide or titanium alkoxide precursor solution, with the increase of H_2O content, concentration of the Ti^{4+} concentration decreased, causing the condensation reaction rate of TiO_6 octahedra to decrease easily forming rutile TiO_2 which has better thermodynamically stability (Fig. 17.7d, e).

Mixed-phase TiO_2 crystals obtained by the sol-gel method are small particles of high purity, but this usually requires long time aging and the particles are easy to agglomerate after high temperature calcination, which may have a significant impact on the photocatalytic activity of TiO_2.

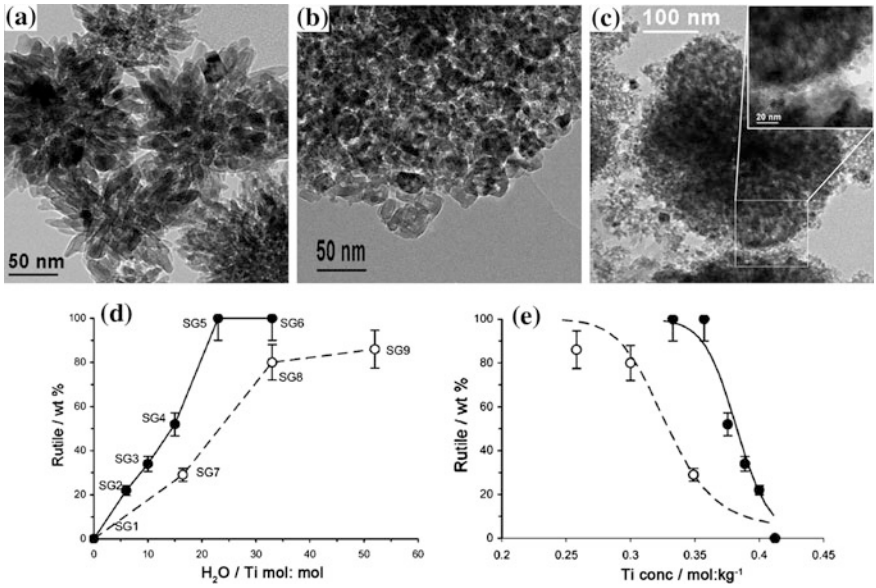

Fig. 17.7 TEM images of **a** pure rutile, **b** pure anatase, and **c** mixed anatase 48 wt% and rutile 52 wt% sample; Plots of rutile content (wt%) in TiO_2 samples: **d** vs. H_2O:Ti molar ratio, **e** vs. titanium concentration [52]

17.3.4 Solvent Mixing and Calcination Method

The solvent mixing and calcination method (SMC method) refers to mixing TiO_2 with different phases in some solvent and then evaporating the solvent completely followed by calcinations at high temperature to make a close contact among different crystal phases. Zachariah et al. [104] synthesized anatase/rutile mixed-phase TiO_2 by the SMC method using anhydrous isopropanol as the solvent. The crystalline size of pure anatase is 10 nm as calculated from the Scherrer equation, and the grain size of pure rutile is 40 nm. In the resultant mixed-phase TiO_2 containing 40 % rutile, the size of anatase is 29 nm, and size of rutile is 47 nm. From Fig. 17.8a, b, pure anatase can be observed consisting of small particles, and the overall particle size is 100–150 nm. The particle size of pure rutile is 300–500 nm (Fig. 17.8c, d). The morphology of the mixed-phase TiO_2 is a mixture of anatase and rutile particles (Fig. 17.8c, f). The phase interface can be seen from the high resolution transmission electron microscopy (HRTEM), indicating there is a close interaction between the two phases. Bojinova et al. [105] prepared an anatase/rutile mixed-phase crystal TiO_2 by the SMC method using ethanol as the solvent. In the mixed-phase TiO_2, the grain size of anatase is 42 nm, and that of rutile is 56 nm, as calculated from the Scherrer formula,. Liu et al. [106] made the anatase small particles adsorbed onto rutile nanorods through a layer-by-layer self-assembly technique, using polystyrene sulfonate (PSS) as a medium and finally the PSS was

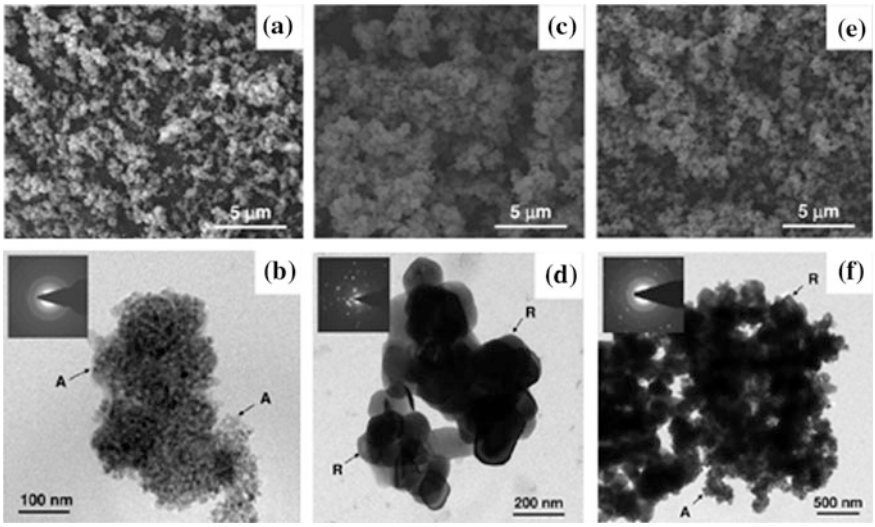

Fig. 17.8 SEM and TEM images of **a**, **b** anatse, **c**, **d** rutile, and **e**, **f** mixed-phase TiO_2 with an optimum rutile content of 40 wt% produced by the SMC method [104]

removed by calcination. The anatase content in the mixed-phase TiO_2 can be controlled by changing the number of loading cycles.

By using the SMC method for the synthesis of mixed-phase TiO_2, the phase content of the product can be regulated easily. However, because of the final calcination process at high temperature, the TiO_2 is easy to agglomerate. In addition, it's usually difficult to achieve uniform mixing of anatase and rutile, leading to products with many pure anatase aggregates as well as pure rutile aggregates. Therefore, the photocatalytic performance of the mixed-phase TiO_2 prepared by this method is subject to limitations.

17.3.5 High-Temperature Calcination Method

The high-temperature calcination method is one of the earliest methods used to synthesize mixed-phase TiO_2, which is mostly used to research the phase transition of TiO_2 [84].

Nair et al. [107] obtained mixed-phase TiO_2 crystal with different anatase and rutile contents by the high-temperature calcination method. They firstly prepared small anatase particles by a sol-gel method and then calcinated the anatase particles under elevated temperatures. It was found that the samples calcined at low temperatures ($T < 600$ °C) remained pure anatase phase. The phase transformation began at 650 °C. When the temperature was raised to 850 °C, the product becomes

pure rutile. In the mixed phase products, the grain size of anatase was 33.66–51.48 nm, and that of rutile was 45.2–60.6 nm, as calculated by the Scherrer formula. As shown in Fig. 17.9, the particle size of anatase was about 100 nm and rutile was about 200 nm; the mixed-phase particle size was between the above two and increased with calcination temperature. The phase transformation is a process of nucleation and growth. However, there is some dispute about the concrete process. Gouma et al. [108] thought that the rutile firstly formed nuclear on the surface of anatase, then extended to the bulk. Zhang et al. [109] verified the phase transformation of anatase-rutile occurred in the bulk firstly, and then spread to the surface with the increase of calcination temperature by UV Raman spectroscopy. The phase's transformation diagram is shown in Fig. 17.10.

The high-temperature calcination method is very simple and can be used to prepare mixed-phase TiO_2 with perfect polymorphs and tunable phase content. However, the hard agglomeration of TiO_2 is serious, and the particles size is large, resulting in limitations of the photocatalytic activity.

Overall, both in the SMC method and the high-temperature calcination method, a high temperature is required to obtain the mixed-phase TiO_2 or close contact between different crystalline forms. As the electron micrographs and XRD results showed, the grain size of crystal after calcination is significantly larger than that of mixed-phase TiO_2 crystals prepared by the in situ method, and the agglomeration is

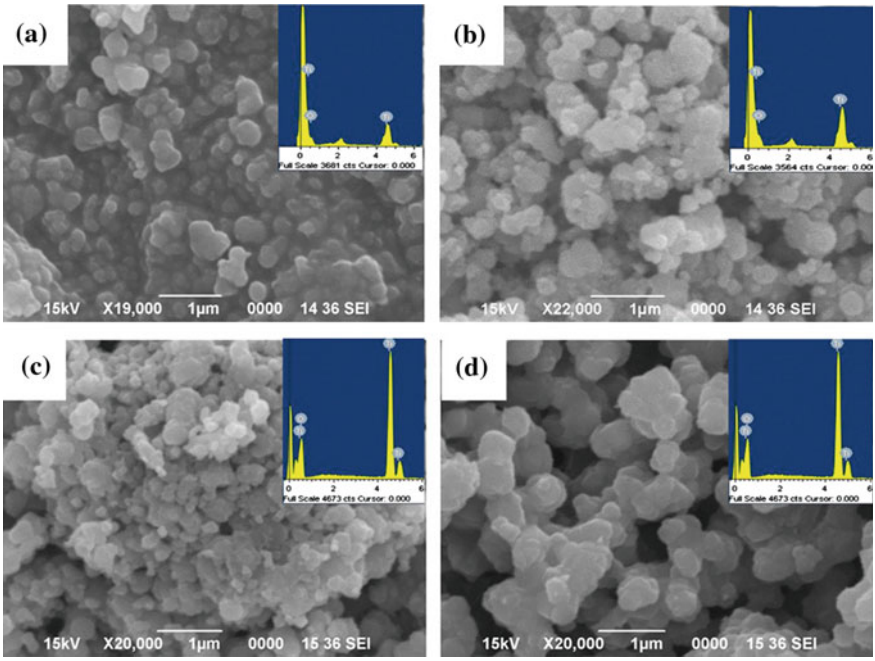

Fig. 17.9 SEM and EDAX images of titania catalysts calcined at different temperature: **a** 600 °C, **b** 700 °C, **c** 750 °C, **d** 800 °C [107]

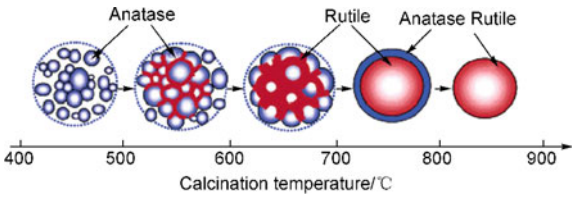

Fig. 17.10 Proposed schemes for the phase transformation of TiO_2 with increasing calcination temperature [109]

Table 17.2 Rate constants for the photocatalytic degradation experiment with mixed-phase TiO_2 synthesized by different methods

Synthesis method	Rate constants/min^{-1}	References
Hydrothermal method	0.019	[53]
Sol-gel method	2.400	[51]
Microemulsion-mediated	0.030	[75]
Solvothermal method		
SMC method	0.023	[77]
Calcination method	0.003	[79]

also serious, all of which can easily cause decrease of photocatalytic activity. Therefore, in recent years, these methods are used relatively less.

The photoctalytic activity rate constants of mixed-phase TiO_2 prepared by different methods are summarized in Table 17.2. From this table, we can see that the reaction rate of TiO_2 synthesized by in situ methods, such as the sol-gel method and microemulsion-mediated hydrothermal method is generally higher than the high-temperature or SMC method. This is because the latter requires high-temperature calcination, resulting in larger particle size and serious agglomeration that reduce the contact area with the degradation target, and impact the photocatalytic activity. However, the reaction rate of mixed-phase TiO_2 prepared by Zheng et al. [54] was small, which may be because high-temperature calcination leads to a hollow structure, which at the same time, decrease the specific surface area and lower the activity. Photocatalytic activities of mixed-phase TiO_2 prepared under different conditions are also influenced by many other factors: product morphology, particle size, crystal proportion.

In addition to the commonly used approaches mentioned above, there are some new methods to prepare mixed-phase TiO_2, for example the microwave heating method [110]. The particle size of TiO_2 synthesized by this method is smaller than that prepared by heating with an oil bath. With the development of new technologies, it is believed that there will be many new methods for synthesizing mixed-phase TiO_2.

17.4 Applications of Mixed-Phase TiO_2 in Photocatalysis

17.4.1 Photocatalytic Hydrogen Production

Hydrogen has been widely recognized as an ideal energy source that could contribute to the replacement of a significant fraction of fossil fuels. However, nowadays the large amount of H_2 demanded is mostly produced from fossil feedstock, mainly by steam reforming of methane. It is therefore mandatory to develop sustainable methods for hydrogen production. Among them, one of the most promising technologies is the photocatalytic hydrogen production, which combines various positive aspects, such as sustainability of the primary energy source (the solar light), the renewability of the starting feedstock and the possible production of by-products with a high added value [111]. And TiO_2 is the most investigated photocatalyst for H_2 production due to its non-toxicity, relatively cheap cost, and excellent stability under the reaction conditions. However, presently, the solar-to-hydrogen energy conversion efficiency of TiO_2 is too low for the technology to be economically sound. The main barriers are the rapid recombination of photo-generated electron-hole pairs as well as backward reaction and the poor activation of TiO_2 by visible light. In response to these deficiencies, many investigators have been conducting research with an emphasis on effective remediation methods like modification of TiO_2 by means of metal loading, metal ion doping, dye sensitization, composite semiconductor, anion doping, and metal ion implantation. In addition to these efforts, mixed-phase TiO_2 have also been explored for hydrogen production [92, 111–115], since multiphasic TiO_2 materials demonstrated higher performances with respect to the correspondent monophasic systems in many photocatalytic processes.

Chen et al. [92] successfully synthesized pure anatase nanoparticles, pure brookite nanoplates, and two-phase anatase/brookite composite by a simple hydrothermal method. Photocatalytic activity of the as-synthesized samples for hydrogen production was investigated in methanol solution. Results have shown that the photocatalytic activity is higher for the two-phase anatase/brookite TiO_2 compared to pure brookite nanoplates, pure anatase nanoparticles and their physically mixed sample, as shown in Fig. 17.11. Moreover, in comparison with the highly active two-phase commercial P25, the synthesized two-phase anatase/brookite TiO_2 is 220 % more active when measured by the H_2 yield per unit area of the photocatalyst surface. Similar results were obtained by Montini et al. [112]. They also prepared TiO_2 nanocomposite with anatase/brookite composition by hydrothermal treatments and the as-prepared anatase/brookite nanocomposites showed higher H_2 production compared to a reference TiO_2 prepared by conventional sol-gel synthesis. Furthermore, they found that the anatase/brookite ratio in the nanocomposite greatly affects the photocatalytic activity in H_2 production.

In addition to the research applying mixed phase anatase/brookite TiO_2 as the photocatalyst for hydrogen production, a great deal of studies have also been done using the mixed phase anatase/rutile TiO_2. Li et al. [113] developed photocatalysts with a tuned anatase/rutile structure by calcination of P25 at different temperatures and

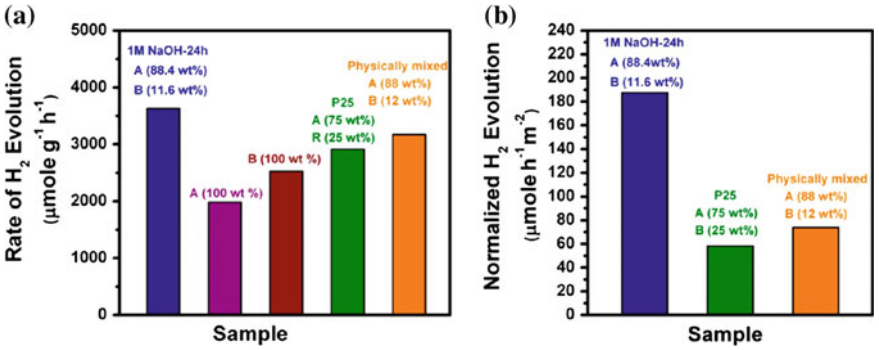

Fig. 17.11 Hydrogen evolved per gram of catalyst per hour under UV−vis irradiation in aqueous methanol solution over 0.3 wt% Pt loaded photocatalysts. A, B and R denote anatase, brookite and rutile respectively [92]

investigated their catalytic activity for hydrogen production by photocatalytic biomass reforming. Surprisingly, they found that the photocatalytic activity of the thermal-treated P25 for hydrogen production can be greatly increased, compared with P25 without any treatment. The overall photocatalytic activity for hydrogen production on thermal-treated P25 can be enhanced up to 3–5 times. It is proposed that the anatase/rutile junction structure is mainly responsible for the improved photocatalytic performance. Their work implies that the photocatalytic performance of TiO_2 could be further improved by elaborately designing the anatase/rutile structure. Similar conclusions were obtained by Amal et al. [114]. They did a systematical study on photocatalytic H_2 evolution over mixed-phase TiO_2 as a function of anatase and rutile phase compositions with methanol as hole scavengers. The TiO_2 nanoparticles they synthesized contain 4–95 mol% anatase, with the remaining being rutile. Synergistic effects in terms of H_2 evolution were observed for a wide range of anatase contents, from 13 to 79 mol%. No synergistic effect was observed for the physically mixed anatase and rutile particles due to insufficient physical contact. Besides the above research on particulate TiO_2 (Fig. 17.12a, b), recently Yu et al. [115] synthesized a kind of anatase/rutile TiO_2 nanofiber photocatalyst (Fig. 17.12b, c). The enhanced H_2 production performance was also observed in the obtained anatase/rutile composite nanofibers. The nanofibers with 45 wt% rutile phase and 55 wt% anatase phase, exhibiting the highest photocatalytic H_2 production rate of 324 mmol h^{-1} and apparent QE of 20.9 % at 365 nm.

Although the research on the mixed-phase TiO_2 of anatase/rutile all demonstrated that the combination of the two phases can greatly enhance the photocatalytic hydrogen production efficiency, the low utilization rate of visible light is still a big problem which limits its practical application. The relatively narrow band gap of rutile allows some visible light absorption; however this is not viable for practical applications. Further efforts have been devoted to expand the visible light absorption of the mixed-phase TiO_2. Keller et al. [116] reported Au modified TiO_2

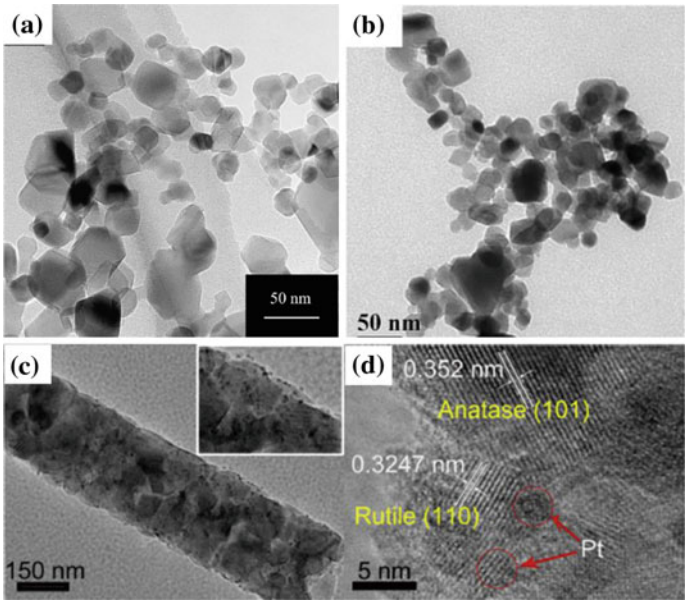

Fig. 17.12 TEM images of particulate anatase and rutile TiO_2; **c**, **d** TEM and HRTEM images of fibrous anatase and rutile TiO_2 [113]

anatase/rutile catalyst (Fig. 17.13) for hydrogen production. They investigated the light absorption of the catalysts with and without Au deposition by UV–Vis light absorption spectra. Before the Au deposition, the samples with rutile phase whose content was higher than that of P25 showed light absorption extended up to 550 nm, but with a relatively low intensity. After Au deposition, the catalysts showed an obvious modification of the absorption properties. This yielded an additional absorption band around 550 nm, which is attributed to a plasmon resonance phenomenon [117] due to collective oscillations of the conduction electrons located on the 6 s orbital of gold and induced by the incident electromagnetic wave. In addition to this plasmon absorption, deposition of gold also shifted the absorption spectrum deeper into the visible light range, in the 380–450 nm regions. This better light absorption in the visible region was demonstrated to contribute to better results for the hydrogen production under simulated solar light. Furthermore, they pointed out that, there are various factors which were crucial to enhance H_2 evolution efficiency: (i) the surface, crystallographic, and porosity properties of the TiO_2 anatase/rutile catalyst, (ii) the anatase/rutile ratio, (iii) the nature and content of the metallic co-catalyst, (iv) the metal-support interactions, and (v) the relative amount of sacrificial reagent. The influence of these different factors was studied in detail by them. In optimized conditions, important H_2 production efficiency (120 μmol min^{-1}) was obtained over days without deactivation and with very low amounts of sacrificial reagent.

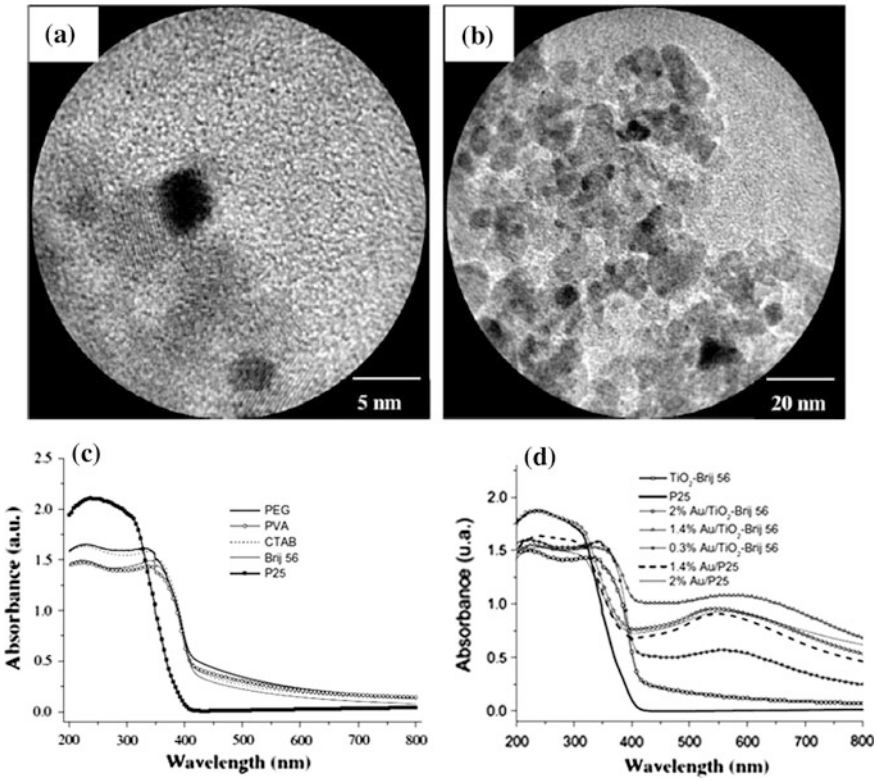

Fig. 17.13 **a**, **b** TEM images of mixed-phase TiO_2 photocatalysts with Au deposition; **c**, **d** Light absorption properties of mixed-phase TiO_2 photocatalysts without and with Au deposition [116]

17.4.2 Photocatalytic Reduction of CO_2 with Water on Mixed-Phase TiO_2

CO_2 is well known to be one of the main causes for the greenhouse effect which leads to global warming. At the same time CO_2 is also a promising carbon resource because it can be converted into various useful chemical compounds and fuels such as CH_4, CH_3OH, HCOOH. Therefore, in order to reduce the emissions of CO_2 and to achieve a sustainable energy future, novel materials and new technologies have been developed to convert CO_2. Besides the methods of solar thermo-chemical conversion and electrochemical reduction of CO_2, solar-activated photocatalytic reduction of CO_2 with water by TiO_2 at room temperature and atmospheric pressure is attractive due to its "green chemistry" and relatively low cost.

During the process of CO_2 photoreduction with H_2O, photo-illumination of the catalyst surface induces the generation of electron-hole pairs in TiO_2. The excited electrons in the conduction band (CB) of TiO_2 could migrate to the surface and

reduce CO_2. Meanwhile, the holes left in the valence band (VB) of TiO_2 could oxidize H_2O into O_2.

The above photocatalytic process has been demonstrated to be closely related to the phase type of TiO_2. Li et al. [118] investigated the CO_2 photoreduction with water vapor on three TiO_2 nanocrystal polymorphs (anatase, rutile, and brookite). Their experimental results showed that, the photocatalytic reduction activity follows the order: anatase > brookite > rutile. The rutile was the least active, mainly due to the fast e^- and h^+ recombination in rutile. They also investigated the photoreduction activity of the TiO_2 catalysts with a helium treatment. The photoreduction data indicated that helium treated catalysts were more active than non-pre-treated ones. And the catalytic activity for production of CO and CH_4 from photoreduction of CO_2 has the order: brookite > anatase > rutile (Fig. 17.14), where brookite exhibited the highest photocatalytic activity. Thus their study also implies that the brookite phase is a promising material for CO_2 reduction, they performed further research on this topic, including the investigation of brookite-containing mixed phases. They prepared bicrystalline anatase/brookite TiO_2 through a hydrothermal method [119]. The as-prepared bicrystalline TiO_2 were also applied for CO_2 photoreduction in the presence of water vapor for production of CO and CH_4. The photocatalytic activities were compared with those of pure anatase, pure brookite, and a commercial anatase/rutile TiO_2 (P25). The results in Fig. 17.15 showed that bicrystalline anatase/brookite was generally more active than pure anatase, brookite, and P25. The bicrystalline mixture with a composition of 75 % anatase and 25 % brookite showed the highest photocatalytic activity, which was nearly twice as high as that of pure anatase (A100) and three times as high as that of single-phase brookite (B100). The higher activity of bicrystalline anatase/brookite is speculated to be ascribed to the interactions between the anatase and brookite nanocrystals.

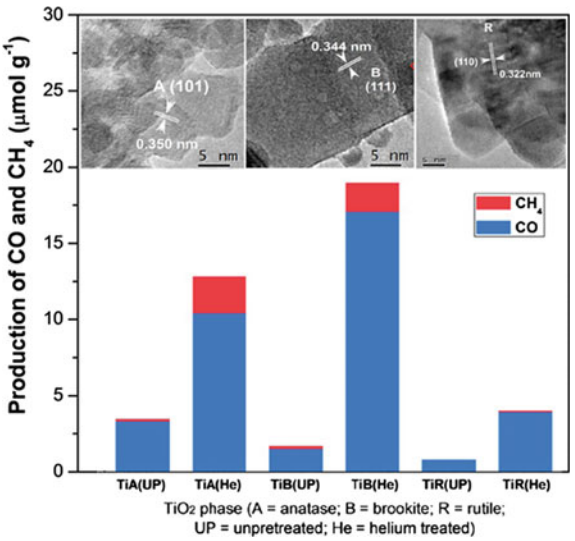

Fig. 17.14 The *top* figures are TEM images of different TiO_2 polymorphs: anatase, brookite and rutile (from *left* to *right*). The *bottom* figure is the production of CO and CH_4 on the three different TiO_2 polymorphs [118]

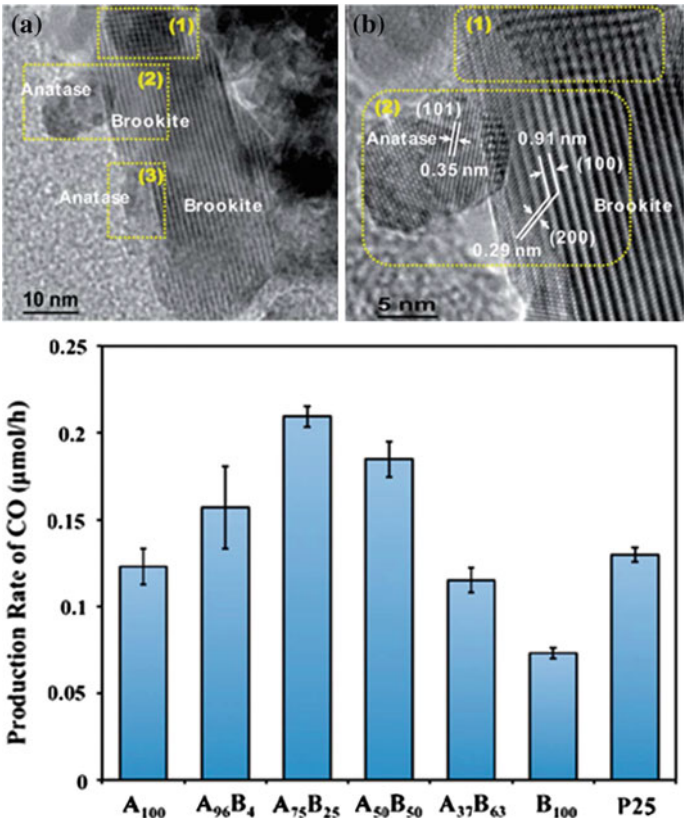

Fig. 17.15 The *top* figures are TEM and HRTEM images of mixed-phase anatase/brookite TiO_2 ($A_{75}B_{25}$). The *bottom* figure is production of CO on various TiO_2 catalysts (A = anatase, B = brookite, the subscript number are the phase fraction of anatase and brookite) [119]

In addition, the anatase-rich bicrystalline anatase/brookite mixtures are superior to anatase/rutile mixtures P25, indicating the interaction between anatase and brookite seems to be more effective than that between anatase and rutile (as in P25) in the photoreduction of CO_2.

17.4.3 Photocatalytic Degradation of Organic Pollutants on Mixed-Phase TiO_2

In 1977, Frank and Bard reported for the first time the photocatalytic decomposition of cyanide by TiO_2 in aqueous medium under sunlight [120]. Since then, the application of TiO_2 for photocatalytic degradation of organic pollutants has gained wide attention due to its effectiveness in degrading and mineralizing the recalcitrant

organic compounds as well as the possibility of utilizing the solar UV and visible-light spectrum. Mixed-phase TiO_2 photocatalysts, which usually have better photocatalytic activity than single-phase TiO_2, have also been widely applied for the degradation of organic pollutants.

Many studies have been carried out to examine the photocatalytic degradation of organic dyes in the presence of mixed-phase TiO_2 as photocatalyst. For instance, methyl blue (MB) were degraded in the aqueous solution by anatase/rutile TiO_2 heterojunction nanoflowers under simulated solar light irradiation [121]. It was found that 72 % of MB could be degraded in 120 min with the mixed-phase catalyst prepared in optimized experimental conditions while only 30 % of MB was degraded in the solution with pure anantase. In addition, the TiO_2 nanoflowers showed excellent stability after 9 cycles under the same conditions. These results suggested that the mixed phase anatase/rutile TiO_2 heterojunction nanoflowers have great potential for the future photodegradation of real dye waste water. Since high surface area is conducive to high catalytic activity, mesoporous mixed-phase anatase/rutile TiO_2 were also prepared [122] (Fig. 17.16a) and applied for the

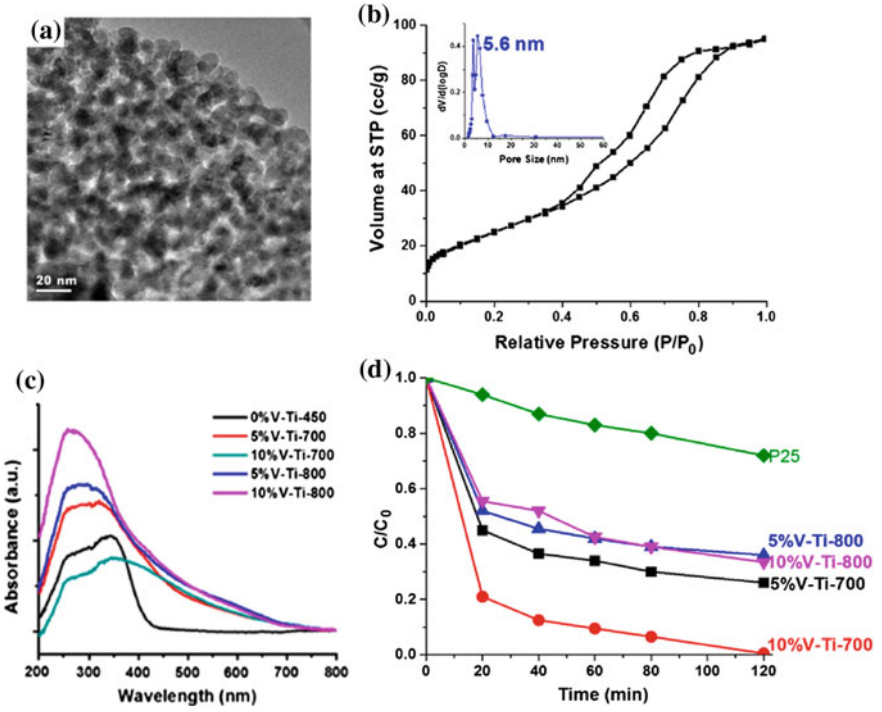

Fig. 17.16 **a** TEM image of mesoporous mixed-phase anatase/rutile TiO_2 (10 %V-Ti-700); **b** N_2 sorption isotherms of 10 %V-Ti-700. The *inset* figure is the BJH desorption pore-size distributions; **c** DR UV−vis spectra for various vanadium doped mixed phase samples; **d** photocatalytic decomposition of 100 mL, 10^{-4} MB dye under visible light in 2 h by using 100 mg of 5 % V-Ti-700, 10 %V-Ti-700, 5 %V-Ti-800, 10 %V-Ti-800, and P25 samples, respectively [122]

photocatalytic degradation of MB. The optimum mesoporous catalyst obtained (10 %V-Ti-700) possess surface area up to 94 m^2 g^{-1} and an average pore size of 5.6 nm (Fig. 17.16b). In addition, the catalyst was in situ doped with vanadium which helped to extend the absorption of TiO_2 to the visible light region (>400 nm) (Fig. 17.16c). As a result, the high surface area, the mixed-phase effect and the vanadium doping qualified the mesoporous mixed-phase anatase/rutile TiO_2 high photocatalytic activity under visible light which are superior to the commercial P25 (Fig. 17.16d).

In addition to the anatase/rutile TiO_2, brookite/rutile TiO_2 were also explored as photocatalysts for the degradation of dyes by Zhang et al. [81]. They synthesize mixed-phase TiO_2 nanocrystals with a tunable brookite-to-rutile ratio by a facile controllable one pot hydrothermal method. The photocatalytic activities of the resulting TiO_2 nanocrystals were examined in the degradation of Rhodamine B under artificial solar light. The TiO_2 nanocrystals with 38 % brookite and 62 % rutile exhibited the highest photocatalytic activity among the as-prepared samples, which was about 6 times that of the commercial P25. Recently,Chen et al. grew anatase grains on the surface of brookite petals resulting in a brookite/anatase TiO_2 hybrid [55], which appeared to have superior photocatalytic activity for the single phase during the degradation of methyl orange (MO) and 2,4-dichlorophenol (2,4-DCP). The hybrid contains 60 % brookite and 40 % anatase and exhibited the highest activity; the degradation rate constants of which are 2.27 and 1.80 times higher than that of the corresponding physically mixed sample for the degradation of MO and 2,4-DCP, respectively. Following this further Ag modification of the brookite/anatase composite [123] was carried out. Ag^0 clusters with an average diameter of ca. 1.5 nm formed on the surface of the mixed-phase composite (Fig. 17.17a, b). The photocatalytic performance of the as-prepared catalysts was evaluated in terms of the degradation of methyl orange (MO). As shown in Fig. 17.17d, the Ag^0-loaded brookite/anatase composite had a higher degradation reaction rate constant than that of the pure anatase and brookite, indicating a better photocatalytic activity. Furthermore, by comparing the results in Fig. 17.17c, d, it can be found that the Ag^0-loaded mixed-phase sample had better catalytic performance than that of Ag free sample. The enhanced photocatalytic reactivity is attributed to the significant improvement in separation of the photo-generated electrons and holes, which can be ascribed to two aspects: (1) synergistic effect of brookite and anatase in the composite, and (2) the schottky barrier at the interface of Ag^0 and TiO_2.

While most research focused on photocatalytic degradation properties of biphasic TiO_2 catalysts, Que et al. explored brookite/anatase/rutile coexisting TiO_2 composite as the photocatalyst [124]. Their results indicated that in the brookite/anatase/rutile coexisting nanopowders, the brookite and anatase phases were crystallized into irregular nanoparticles <20 nm in diameter, whereas the rutile phase was crystallized into single-crystalline nanorods $\sim$20 nm in diameter and 100–500 nm in length, as shown in Fig. 17.18a. This triphasic TiO_2 catalyst was demonstrated to have better photocatalytic activity during degradation of methyl orange than the biphasic commercial P25 under irradiation of UV light. The sample

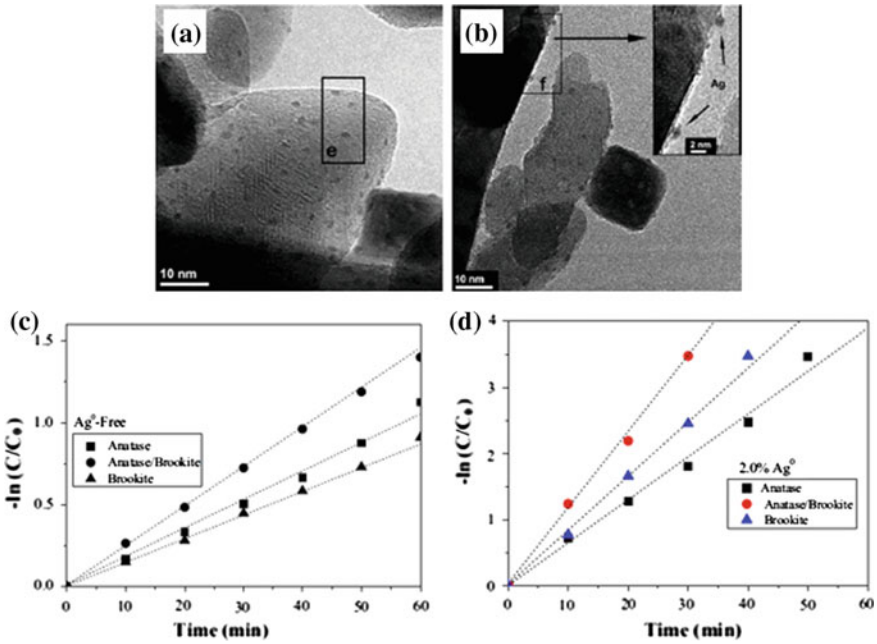

Fig. 17.17 TEM images of 2.0 % Ag^0-TiO_2 (brookite/anatase) (**a**, **b**); photocatalytic degradation of MO with Ag-free (**c**) and 2.0 % Ag^0-loaded (**d**) TiO_2 with different crystal phase composition under UV irradiation [55]

with 29.9 % anatase, 27.9 % brookite, 42.2 % rutile (referred as T2) was shown to have the highest photocatalytic activity, yielding over 90 % bleaching of methyl orange solution in 20 min (Fig. 17.18b). The degradation rate constant k of this sample was 0.10180 min^{-1}, almost twice as high as that of P25 (k = 0.05397 min^{-1}). In addition, recycle experiments of the photocatalyst were also carried out by using the best photocatalyst sample T2 as shown in Fig. 17.18c. It can be seen that after five recycles, the photocatalytic activity of the sample shows only a slight loss, indicating a good stability of the triphasic TiO_2 catalyst in the photocatalytic degradation process. Similarly, Shao et al. also developed brookite/anatase/rutile triphasic TiO_2 and the catalyst was demonstrated to have excellent photocatalytic performance in the degradation of methylene blue solutions.

Apart from dyes, some other organic compounds have also been used as the model pollutants in the mixed-phase TiO_2 photocatalysis system. For example, phenol and its derivatives have been widely studied as photodegradation target molecules, since they are considered to be one type of primary pollutants due to their danger to organisms at low concentrations [125]. Lu et al. [126] prepared a series of TiO_2 samples with different anatase-to-rutile ratios, and studied the role of crystal phase in photocatalytic oxidation of phenol in water. They found that samples with higher anatase-to-rutile ratios have higher activities for phenol

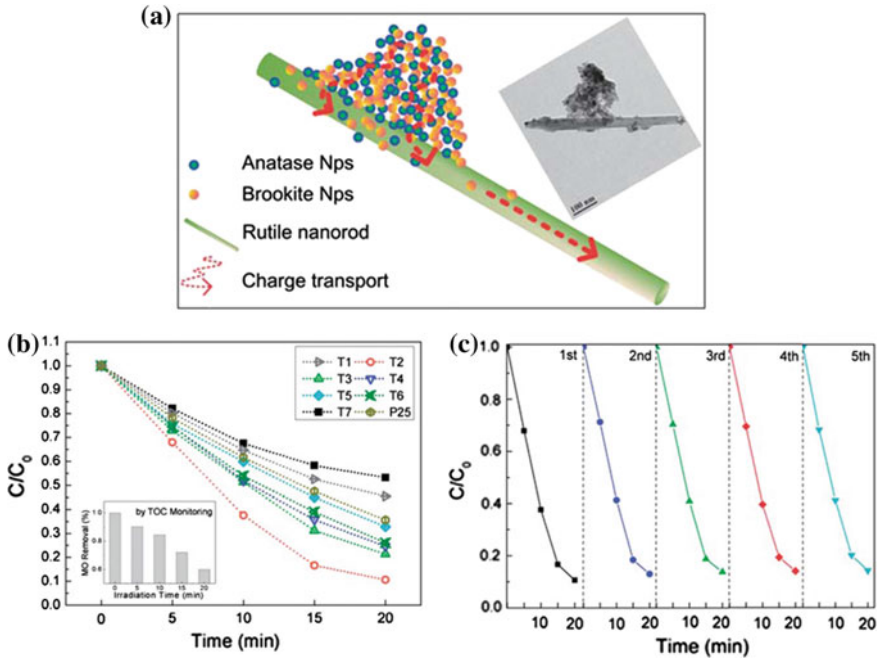

Fig. 17.18 **a** Scheme and TEM image of the brookite/anatase/rutile nanocomposites; **b** Photocatalytic degradation of the MO aqueous solution by using the brookite/anatase/rutile nanocomposites synthesized with various reagent ingredients, and the *inset* shows the removal of MO monitored by TOC with the sample T2 as photocatalysts; **c** Cycling degradation *curves* of the brookite/anatase/rutile coexisting nanocomposites (sample T2) [124]

degradation. Tian et al. [127] reported Cr-doped TiO_2 (Cr-TiO_2) nanoparticles with anatase and rutile bicrystalline phases for the photocatalytic degradation of 2,4-dichlorophenol (2,4-DCP). It was revealed that Cr^{3+} doping can not only effectively extend the visible light response of TiO_2 (Fig. 17.19a) but also promote the anatase-to-rutile transformation. The photocatalytic activities of different Cr-TiO_2 photocatalytsts were evaluated in terms of the photocatalytic degradation of 2, 4-dichlorophenol (2, 4-DCP) under visible light irradiation (Fig. 17.19b). They found appropriate Cr^{3+} doping can significantly enhance the visible-light photocatalytic activity of TiO_2, which is attributed to the improvement of visible light response as well as suitable anatase-to-rutile ratio. In addition, excess Cr^{3+} doping is detrimental to the improvement of visible light photocatalytic activity, due to the formation of Cr_2O_3 clusters as well as too high a rutile content.

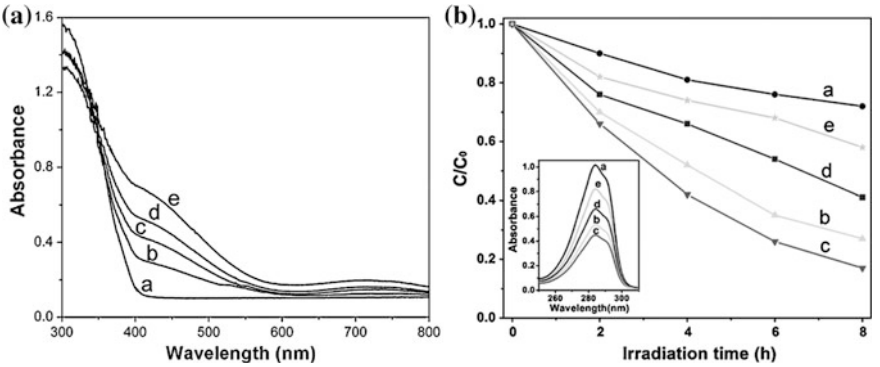

Fig. 17.19 **a** UV-vis DRS and **b** degradation curves of 2, 4-DCP over undoped TiO_2 and different Cr-TiO_2 samples under visible light irradiation: **a** undoped TiO_2, **b** 0.5 % Cr-TiO_2, **c** 1 % Cr-TiO_2, **d** 2 % Cr-TiO_2, and **e** 5 % Cr-TiO_2. The *inset* is the absorption spectra of 2, 4-DCP over different samples after visible light irradiation for 8 h [127]

17.5 Mechanism of the Enhanced Photocatalytic Activities by the Mixed-Phase TiO_2 Photocatalysis

Generally, most of the photo-generated electrons and holes of the single-phase TiO_2 will recombine in the bulk, and only a small amount of them can migrate to the surface to take part in the oxidation-reduction reactions with absorbed molecules, leading to relatively low photocatalytic efficiency. In 1991, Bickley et al. [128] first proposed the mechanism of enhanced photocatalytic activity of P25 which is composed of 80 % anatase and 20 % rutile. They proved that the mixed-phase structure of P25 is an anatase structure coated with a layer of rutile film by TEM. By evaluating the photocatalytic activities, they found that the photocatalytic activity of the mixed-phase TiO_2 was better than the activity of any other single-phase TiO_2 photocatalyst. Because the anatase and rutile have different band gaps, a bending band is generated on the interface of the two phases, as shown in Fig. 17.20. Under light irradiation, the photo-generated electrons migrate from rutile phase to anatase phase, while the holes migrate from anatase phase to rutile phase, so that the electrons and holes can be separated effectively, causing the mixed-phase P25 to have a high photcatalytic activity. Meanwhile, they speculated that the mechanism of the enhanced photocatalytic activity of mixed-phase TiO_2 is actually more complex and requires further study. Subsequently, researchers have studied the mobility direction of the photo-generated carriers, the molecular dynamics characterizations of the mixed-phase interface [129], the band structure of mixed-phase TiO_2 [130, 131], the suitable phase proportion in the mixed-phase TiO_2 and so on.

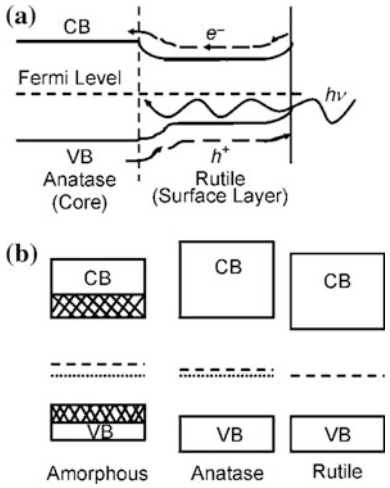

Fig. 17.20 Schematic band structure diagrams of P25 [128]

In 1995, Datye et al. [132]. refuted the view of Bickley et al. [128] on the mixed-phase crystal structure in P25 by X-ray diffraction (XRD) and high-resolution transmission electron microscopy (HRTEM) techniques. Their characterization results showed that the mixed-phase P25 consists of individual single crystal particles of the anatase and the rutile phases of titania rather than particles of anatase covered by a layer of rutile. This view was confirmed by Zhang et al. [133] and Ohno et al. [134]. But they did not pursue further research on the mechanism of the enhanced photocatalytic performance resulted from the mixing of two phases.

In 2002, Kawahara et al. [135] designed a film model to study the migration direction of the photo-generated electrons and holes in anatase/rutile mixed-phase crystal under light irradiation. In their experiments, the mixed-phase crystal TiO_2 film was immersed into an $AgNO_3$ solution, and it was exposed to light over a period of time under an argon atmosphere. Experimental results showed that there were a large number of Ag particles on the surface of the rutile phase. It is possible that Ag^+ caused a reduction reaction on the rutile surface, indicating that the photo-generated electrons migrated from the conduction band of anatase to rutile (Fig. 17.21).

In 2003, Sun et al. [137, 138] deposited Pt on P25 for the photocatalytic degradation of phenol. However, they found that loading P25 with Pt didn't help to increase phenol decomposition and total carbon removal rates. In addition, they found that Pt appeared on the surface of anatase. Therefore, they proposed a charge separation mechanism for the mixed-phase P25 as "contact of the two phases causing the bending of the conduction band resulting in the holes in anatase transferring to rutile, while the electrons cannot transfer from anatase to rutile", as shown in Fig. 17.22. As a result, holes were concentrated in rutile and electrons were left in the anatase particles, which indicated that oxidation happens mostly on rutile and reduction mostly on anatase, thus the Pt deposition on anatase cannot increase its photo efficiency for phenol oxidation in water.

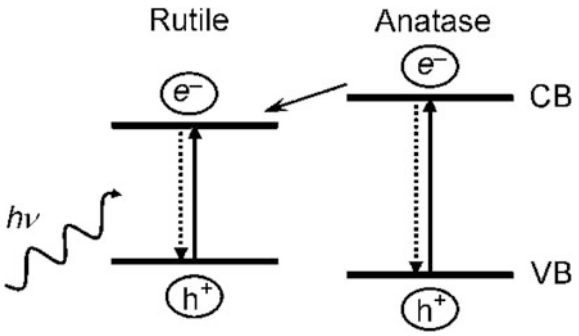

Fig. 17.21 A proposed schematic illustrations showing the migration of the electron transfer from anatase to rutile [135, 136]

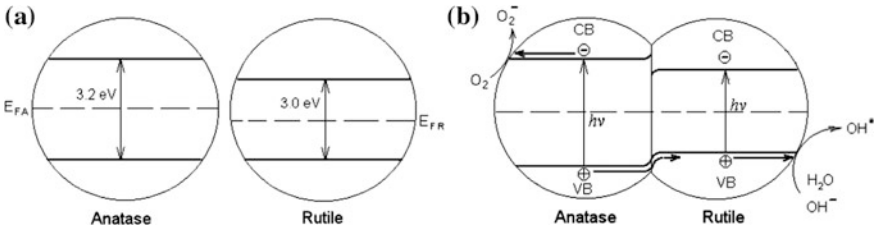

Fig. 17.22 **a** Band structure before anatase and rutile contact each other; **b** Band structure and the separation of photo-generated charge carriers after anatase and rutile contact each other [137]

In the same year, Hurum et al. [51] characterized the charge separation process of P25 by electron paramagnetic resonance (EPR). When P25 mixed-phase crystal was excited by visible light, due to the wide band gap of anatase, no electrons and holes were generated. However, in electron paramagnetic resonance spectroscopy, the electrons trapping sites were found on anatase surface, and it could be concluded that the electrons in rutile generated by visible light excitation transferred to the lower energy anatase lattice trapping sites, leading to a more stable charge separation and enhancing the photocatalytic activity of P25 (Fig. 17.23). Thereafter, this mechanism was confirmed by Liu et al. [139] through the photocatalytic activity experiments of anatase/rutile mixed-phase TiO_2 nanotubes. EPR spectroscopy is a new characterization method developed in recent years, which is a spectroscopic method to detect the unpaired electrons in the sample. Since then, researchers have began to characterize the migration of photo-generated electrons and holes in the mixed-phase TiO_2 using the EPR technique [140].

In 2006, Wang et al. [141] proposed an "antenna mechanism" to explain the mechanism of enhanced photocatalytic activity in mixed crystal phases. The specific mechanism is as follows: in the photocatalytic degradation process, TiO_2 absorbs light to produce photo-generated electrons and holes, which then take part

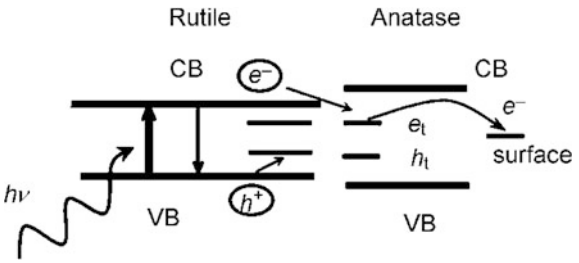

Fig. 17.23 A proposed schematic illustrations showing the charge separation using EPR [51]

in the oxidation-reduction reactions with the target molecules adsorbing on the catalyst's surface; However, the depth in liquid which light can reach is limited, so that the deeper the liquid molecules, the less light they receive. Therefore, the particles irradiated by light can absorb photo energy, this energy can then be transferred from to particles deeper in the liquid, finally oxidation-reduction reaction takes place on the particles which light cannot reach, enhancing the photocatalytic activity. In the process of photo energy being transferred to the photocatalyst deeper in the liquid, the long-chain particles act as an antenna system transferring the photon energy from the location of light absorption to the location of reaction, thus this is called an "antenna mechanism" (Fig. 17.24).

However, the research objects of the above-mentioned theoretical models are all P25 which has a fixed phase ratio of anatase and rutile. Because mixed-phase TiO_2 with different phase ratios have different photocatalytic activities, none of these existing models can adequately explain the physical phenomenon responsible for the existence of an optimum phase content in mixed-phase nanocrystalline TiO_2 corresponding to the maximum photocatalytic activity. Therefore, further research is needed to investigate the photocatalytic mechanism of mixed-phase TiO_2 with different phase ratios.

In 2008, Zachariah et al. [104] proposed a new mechanism model, which takes the factors of crystallite size distribution and phase composition into account. This mechanism overcomes the limitations of the existing models proposed earlier in the literature in terms of explaining the phenomenon of an existing optimal phase ratio in the mixed-phase TiO_2 for the best photocatalytic activity. The mechanism is based on the charge separation mechanism proposed by Sun et al. [137]. In the mechanism, when the size of nano TiO_2 is identical (Fig. 17.25a), the band gap of

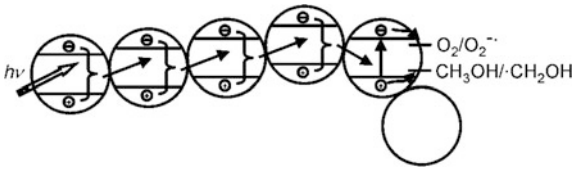

Fig. 17.24 Antenna effect by network structure leading to enhanced photocatalytic activity [141]

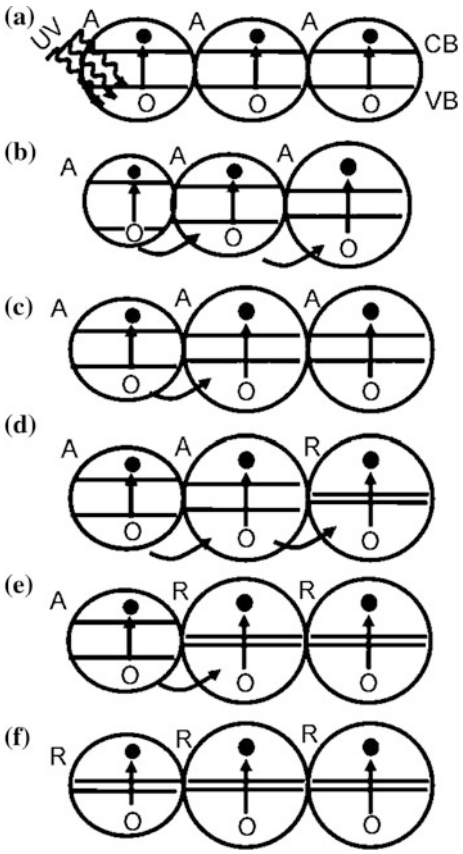

Fig. 17.25 The newly proposed mechanism model based on the band-gap variation in the connected nanocrystallites as a function of the size distribution and the phase involved [104]. A, R, CB, and VB represent anatase-TiO_2, rutile-TiO_2, the conduction band, and the valence band, respectively [104]

adjacent anatase crystallites is the same, so there is no driving force for the migration of photo-generated holes, resulting in high recombination rate of photo-generated charges and low photocatalytic activity. If the sizes of anatase crystallite are different and are below the critical size (Fig. 17.25b, c), the band gaps of the connected crystallites would depend on their size. Thus, photo-generated holes in one crystallite can easily escape into the other leading to effective charge separation. When a small amount of rutile was mixed with anatase (Fig. 17.25d), due to the different band gap, photo-generated holes will transfer from anatase to rutile, so that the photocatalytic activity is further enhanced. However, if the rutile content exceeds a certain amount, the migration of photo-generated holes in mixed-phase crystal TiO_2 is limited (Fig. 17.25e), and the photocatalytic activity begins to decline. Given that the crystallite sizes of pure rutile are above the critical size (Fig. 17.25f), their band gap values are the same, then the migration of photogenerated holes does not occur, and the photocatalytic activity is minimum. The key point of this mechanism is that whether the TiO_2 is mixed-phase crystalline or

single crystalline, as long as the band gap values are different, the photo-generated electron-hole pairs will be separated, thereby improving the photocatalytic activity.

In summary, the above mechanisms for the enhanced photocatalytic performance of mixed-phase TiO_2 all involve the migration behavior of photo-generated electrons and holes. In these mechanisms, the mixed-phase crystal structure enables the effective separation of photo-generated electrons and holes, while the specific paths of migration are still controversial. The determining factors for photocatalytic activity of mixed-phase crystal TiO_2 include grain size, structural forms (core-shell structure, cladding structure, random composite, etc.), phase composition. These factors lead to the emergence of bending band, trapping sites and other phenomena in the mixed-phase crystal. Therefore, under different experimental conditions, the obtained mixed-phase TiO_2 differ in photocatalytic mechanism, so further research is still required.

17.6 Conclusion and Outlook

Research in the synthetic methods and applications in photocatalysis of mixed-phase TiO_2 have made great progress since the discovery of photocatalytic water splitting and degradation of organic pollutants by TiO_2 nanomatrials in the 1970s. The superior photocatalytic performance of mixed-phase TiO_2 to single-phase TiO_2 has been well received and the mechanism of the enhanced photocatalytic activities by the mixed-phase TiO_2 photocatalysis has also been widely studied. However, there are still many problems remaining to be resolved. For example, (1) Particulate mixed-phase TiO_2 nanomaterials are prone to agglomeration, which will greatly decrease the photocatalytic activity and hinder the further development of the materials; (2) Although the relatively narrow band gap of rutile extends the absorption of the mixed-phase TiO_2 to some of the visible light range, it is still insufficient to utilize all visible light from sun light, limiting its application in photocatalysis; (3) Although researchers all agree that the mixed-phase crystal structure enables the effective separation of photogenerated electrons and holes, thereby enhancing the photocatalytic activity, there is much controversy about the mobility direction of photo-generated electrons and holes. Further research is essential to confirm the mechanism of the enhanced photocatalytic activity of mixed-phase TiO_2. Therefore, developing mixed-phase TiO_2 nanomaterials and combining other advantageous structures (such as hierarchical structure), enhancing the visible light utilization, and exploring the mechanism by newly developed characterization techniques will continue to be the challenges and hot research topics in this area.

Although mixed-phase crystal TiO_2 has been studied for decades, it is still a popular topic due to its excellent photocatalytic activity. Nowadays, with increasingly serious energy and environmental problems, the applications of mixed-phase TiO_2 is anticipated to attract considerable attention.

References

1. A. Fujishima, K. Honda, Nature **238**, 37–38 (1972)
2. J.H. Carey, J. Lawrence, T. Hm, Bull. Environ. Contam. Toxicol. **16**, 697–701 (1977)
3. S.N. Habisreutinger, S.L. Mende, J.K. Stolarczyk, Angewandte Chemie **52**, 7372–7408 (2013)
4. H. Ke, K.C.D. Robson, P.G. Johansson, C.P. Berlinguette, G.J. Meyer, J. Am. Chem. Soc. **134**, 8352–8355 (2012)
5. Q. Guo, C. Xu, Z. Ren, W. Yang, Z. Ma, D. Dai, H. Fan, T.K. Minton, X. Yang, J. Am. Chem. Soc. **134**, 2827–2830 (2012)
6. B. Tian, F. Chen, J. Zhang, M. Anpo, J. Colloid Interface Sci. **303**, 142–148 (2006)
7. M. Tomkiewicz, G. Dagan, Z. Zhu, Res. Chem. Intermed. **20**, 701–710 (1994)
8. S. Zhu, G. Xie, X. Yang, Z. Cui, Mater. Res. Bull. **48**, 1961–1966 (2013)
9. T. Beuvier, M. Richard-Plouet, G.M. Mancini-Le, T. Brousse, O. Crosnier, L. Brohan, Inorg. Chem. **49**, 8457–8464 (2010)
10. X. Xin, M. Scheiner, M. Ye, Z. Lin, Langmuir **27**, 14594–14598 (2011)
11. E. Hosono, S. Fujihara, H. Imai, I. Honma, I. Masaki, H. Zhou, ACS Nano **1**, 273–278 (2007)
12. A.K. Sinha, S. Jana, S. Pande, S. Saha, A. Pal, T. Pal, S. Sarkar, M. Pradhan, M. Basu, Cryst. Eng. Comm. **7**, 1210–1212 (2009)
13. Q.Q. Cheng, Y. Cao, L. Yang, P.P. Zhang, K. Wang, H.J. Wang, Mater. Res. Bull. **46**, 372–377 (2011)
14. Y. Wang, L. Zhang, K. Deng, X. Chen, Z. Zou, J. Phys. Chem. C **111**, 2709–2714 (2007)
15. J. Wei, J. Yao, X. Zhang, W. Zhu, H. Wang, M.J. Rhodes, Mater. Lett. **61**, 4610–4613 (2007)
16. Y. Hu, Angew. Chem. Int. Ed. **51**, 12410–12412 (2012)
17. J.K. Oh, J.K. Lee, H.S. Kim, S.B. Han, K.W. Park, Chem. Mater. **22**, 1114–1118 (2009)
18. M. Ye, H.Y. Liu, C. Lin, Z. Lin, Small **9**, 312–321 (2013)
19. S. Peng, S. Ding, J. Yuan, W.L. Xiong, D.H. Kim, ACS Nano **5**, 7617–7626 (2011)
20. E. Lioz, G. Peng, X. Zhaosheng, P. Qin, C. Aravind Kumar, L. Bin, M.K. Nazeeruddin, G.T. Michael, J. Am. Chem. Soc. (2012)
21. W. Guo, C. Xu, X. Wang, S. Wang, C. Pan, C. Lin, Z. Wang, J. Am. Chem. Soc. **134**, 4437–4441 (2012)
22. Y.Q. Wang, G. Lin, Y.G. Guo, L. Hong, X.Q. He, S. Tsukimoto, Y. Ikuhara, L.J. Wan, J. Am. Chem. Soc **134**, 7874–7879 (2012)
23. S.S.K. Lee, P. Schmuki, J. Am. Chem. Soc. **134**, 11316–11318 (2012)
24. W.N. Wang, W.J. An, B. Ramalingam, S. Mukherjee, D.M. Niedzwiedzki, S. Gangopadhyay, P. Biswas, J. Am. Chem. Soc. **134**, 11276–11281 (2012)
25. S.A.K. Leghari, S. Sajjad, F. Chen, J. Zhang, Chem. Eng. J. **166**, 906–915 (2011)
26. F. Chen, W. Zou, W. Qu, J. Zhang, Catal. Commun. **10**, 1510–1513 (2009)
27. M. Xing, J. Zhang, F. Chen, Appl. Catal. B **89**, 563–569 (2009)
28. T.H. Kim, C. Gómez-Solís, E. Moctezuma, S.W. Lee, Res. Chem. Intermed. **40**, 1595–1605 (2014)
29. F. Zuo, L. Wang, T. Wu, Z. Zhang, D. Borchardt, P. Feng, J. Am. Chem. Soc. **132**, 11856–11857 (2010)
30. J.K. Yong, H.L. Mi, H.J. Kim, G. Lim, Y.S. Choi, N.G. Park, K. Kim, I.L. Wan, Adv. Mater. **21**, 3668–3673 (2009)
31. S. Liu, Q. Li, C. Hou, X. Feng, Z. Guan, J. Alloy. Compd. **575**, 128–136 (2013)
32. M. Cai, X. Pan, W. Liu, J. Sheng, X. Fang, C. Zhang, Z. Huo, H. Tian, S. Xiao, S. Dai, J. Mater. Chem. A **15**, 4885–4892 (2013)
33. M.S. Liang, C.C. Khaw, C.C. Liu, S.P. Chin, J. Wang, H. Li, Ceram. Int. **39**, 1519–1523 (2013)

34. H. Kim, H.H. Yun, G. Cho, D. Kim, N. Lim, M. Pyo, Electrochim. Acta **56**, 9476–9481 (2011)
35. C. Zhang, Y. Huang, S. Chen, H. Tian, L.E. Mo, L. Hu, Z. Huo, F. Kong, Y. Ma, S. Dai, J. Phys. Chem. C **116**, 19807–19813 (2012)
36. E.G. Bae, H. Kim, Y.H. Hwang, K.S. Sohn, M. Pyo, J. Mater. Chem **22**, 551–556 (2011)
37. A.A. Ashkarran, M. Ghavamipour, H. Hamidinezhad, H. Haddadi, Res. Chem. Intermed. (2014)
38. M. Haruta, B.S. Uphade, S. Tsubota, A. Miyamoto, Res. Chem. Intermed. **24**, 329–336 (1998)
39. B. Tian, J. Zhang, T. Tong, F. Chen, Appl. Catal. B **79**, 394–401 (2008)
40. Y. Wu, H. Liu, J. Zhang, F. Chen, J. Phys. Chem. C **113**, 14689–14695 (2009)
41. W. Wang, J. Zhang, F. Chen, M. Anpo, D. He, Res. Chem. Intermed. **36**, 163–172 (2010)
42. W. Yan, C. Feng, Z. Min, J. Yang, Z. Zhang, Appl. Catal. B **100**, 84–90 (2010)
43. C. Feng, Y. Wang, J. Zhang, L. Yu, D. Li, J. Yang, Z. Zhang, Appl. Catal. B Environ. **113–114**, 61–71 2012
44. A. Charanpahari, S.S. Umare, S.P. Gokhale, V. Sudarsan, B. Sreedhar, R. Sasikala, Appl. Catal. A **443**, 96–102 (2012)
45. B. Tian, C. Li, F. Gu, H. Jiang, Catal. Commun. **10**, 925–929 (2009)
46. P. Zhang, C. Shao, X. Li, M. Zhang, X. Zhang, Y. Sun, Y. Liu, J. Hazard. Mater. **237–238**, 331–338 (2012)
47. Z.H. Zhang, Y. Yuan, L.H. Liang, Y.X. Cheng, G.Y. Shi, L.T. Jin, J. Hazard. Mater. **158**, 517–522 (2008)
48. G. Chattopadhyaya, D.G. Macdonald, N.N. Bakhshi, J.S.S. Mohammadzadeh, A.K. Dalai, Catal. Lett. **108**, 1–5 (2006)
49. M. Yang, Y. Men, S. Li, G. Chen, Appl. Catal. A **433**, 26–34 (2012)
50. S. Ren, R. Bechstein, L. S03, R.T. Vang, M. Sillassen, B. Esbjörnsson, A. Palmqvist, F. Besenbacher, J. Phys. Chem. C **115**, 24287–24292 (2011)
51. D.C. Hurum, A.G. Agrios, K.A. Gray, T. Rajh, M.C. Thurnauer, J. Phys. Chem. B **107**, 4545–4549 (2003)
52. R. Scotti, I.R. Bellobono, C. Canevali, C. Cannas, M. Catti, M. D'Arienzo, A. Musinu, S. Polizzi, M. Sommariva, A. Testino, Chem. Mater. **20**, 4051–4061 (2008)
53. V. Puddu, H. Choi, D.D. Dionysiou, G.L. Puma, Appl. Catal. B **94**, 211–218 (2010)
54. R. Zheng, X. Meng, F. Tang, Appl. Surf. Sci. **255**, 5989–5994 (2009)
55. Y. Jiao, F. Chen, B. Zhao, H. Yang, J. Zhang, Colloids Surf., A **402**, 66–71 (2012)
56. A.D. Paola, G. Cufalo, M. Addamo, M. Bellardita, R. Campostrini, M. Ischia, R. Ceccato, L. Palmisano, Colloids Surf., A **317**, 366–376 (2008)
57. W. Li, C. Liu, Y. Zhou, Y. Bai, X. Feng, Z. Yang, L. Lu, X. Lu, K.Y. Chan, J. Phys. Chem. C **112**, 20539–20545 (2008)
58. D. Hanaor, C. Sorrell, J. Mater. Sci. **46**, 855–874 (2011)
59. J.A. Gamboa, D.M. Pasquevich, J. Am. Ceram. Soc. **75**, 2934–2938 (1992)
60. X.Z. Ding, Y.Z. He, J. Mater. Sci. Lett. **15**, 320–322 (1996)
61. J. Muscat, V. Swamy, N.M. Harrison, Phys. Rev. B **65**, 392–397 (2002)
62. T. Arlt, M. Bermejo, M.A. Blanco, L. Gerward, J.Z. Jiang, J. Staun Olsen, J.M. Recio, Phys. Rev. B **61**, 14414–14419 (2000)
63. R. Ren, Z. Yang, L.L. Shaw, J. Mater. Sci. **35**, 6015–6026 (6012) (2000)
64. N.A. Dubrovinskaia, L.S. Dubrovinsky, R. Ahuja, V.B. Prokopenko, V. Dmitriev, H.P. Weber, J.M. Osorio-Guillen, B. Johansson, Phys. Rev. Lett. **87**, 455–475 (2001)
65. U. Diebold, Surf. Sci. Rep. **48**, 53–229 (2003)
66. M. Yan, F. Chen, J. Zhang, M. Anpo, J. Phys. Chem. B, **109** (2005)
67. Y. Li, T.J. White, S.H. Lim, J. Solid State Chem. **177**, 1372–1381 (2004)
68. A.R. Khataee, M.B. Kasiri, J. Mol. Catal. A: Chem. **328**, 8–26 (2010)
69. N. Daneshvar, M.H. Rasoulifard, A.R. Khataee, F. Hosseinzadeh, J. Hazard. Mater. **143**, 95–101 (2007)
70. M.P. Moret, R. Zallen, D.P. Vijay, S.B. Desu, Thin Solid Films **366**, 8–10(13) (2000)

71. R.D. Shannon, J.A. Pask, J. Am. Ceram. Soc. **48**, 391–398 (1965)
72. M. Batzill, E.H. Morales, U. Diebold, Phys. Rev. Lett. **96** (2006)
73. G. Oskam, A. Nellore, R.L. Penn, P.C. Searson, J. Phys. Chem. B **107**, 1734–1738 (2003)
74. H. Zhang, J.F. Banfield, J. Mater. Chem. **9**, 2073–2076 (1998)
75. J.G. Li, T. Ishigaki, X. Sun, J. Phys. Chem. C **111**, 4969–4976 (2007)
76. R.I. Bickley, T. Gonzalez-Carreno, J.S. Lees, L. Palmisano, R.J.D. Tilley, J. Solid State Chem. **92**, 178–190 (1991)
77. S.-K. Lee, P.K.J. Robertson, A. Mills, D. McStay, J. Photochem. Photobiol. A **122**, 69–71 (1999)
78. S.J. Tsai, S. Cheng, Catal. Today **33**, 227–237 (1997)
79. T. Ohno, K. Sarukawa, M. Matsumura, J. Phys. Chem. B **105**, 2417–2420 (2001)
80. T. Ozawa, M. Iwasaki, H. Tada, T. Akita, K. Tanaka, S. Ito, J. Colloid Interface Sci. **281**, 510–513 (2005)
81. H. Xu, L. Zhang, J. Phys. Chem. C **113**, 1785–1790 (2009)
82. R.R. Bacsa, J. Kiwi, Appl. Catal. B **16**, 19–29 (1998)
83. K.Y. Jung, S.B. Park, H.D. Jang, Catal. Commun. **5**, 491–497 (2004)
84. S. Leghari, S. Sajjad, F. Chen, J. Zhang, Chem. Eng. J. **3**, 906–915 (2011)
85. J. Zhu, W. Zheng, B. He, J. Zhang, M. Anpo, J. Mol. Catal. A: Chem. **216**, 35–43 (2004)
86. Y. Wu, M. Xing, J. Zhang, J. Hazard. Mater. **192**, 368–373 (2011)
87. J. Ng, X. Wang, D.D. Sun, Appl. Catal. B **110**, 260–272 (2011)
88. J. Ovenstone, K. Yanagisawa, Chem. Mater. **11**, 2770–2774 (1999)
89. G. Li, S. Ciston, Z.V. Saponjic, L. Chen, N.M. Dimitrijevic, T. Rajh, K.A. Gray, J. Catal. **253**, 105–110 (2008)
90. M. Fehse, F. Fischer, C. Tessier, L. Stievano, L. Monconduit, J. Power Sources **231**, 23–28 (2013)
91. Y. Zhang, J. Chen, X. Li, Catal. Lett. **139**, 129–133(125) 2010
92. Q. Tay, X. Liu, Y. Tang, Z. Jiang, T.C. Sum, Z. Chen, J. Phys. Chem. C **117**, 14973–14982 (2013)
93. H. Zhang, J.F. Banfield, J. Phys. Chem. B **104**, 3481–3487 (2000)
94. X. Shen, B. Tian, J. Zhang, Catal. Today **201**, 151–158 (2013)
95. B. Zhao, F. Chen, Q. Huang, J. Zhang, Chem. Commun. **34**, 5115–5117 (2009)
96. L.M. Zhao, Z.J. Zhang, S.Y. Zhang, P. Cui, W. Shi, B. Zhao, P. Cheng, D.Z. Liao, S.P. Yan, Cryst. Eng. Comm. **3**, 907–913 (2011)
97. B. Zhao, F. Chen, Y. Jiao, J. Zhang, J. Mater. Chem. **20**, 7990–7997 (2010)
98. X. Shen, J. Zhang, B. Tian, M. Anpo, J. Mater. Sci. **47**, 5743–5751 (2012)
99. H. Cheng, J. Ma, Z. Zhao, L. Qi, Chem. Mater. **7**, 663–671 (1995)
100. G. Li, K.A. Gray, Chem. Mater. **19**, 1143–1146 (2007)
101. S. Lei, W. Duan, J. Environ. Sci. **20**, 1263–1267 (2008)
102. M. Wu, J. Long, A. Huang, Y. Luo, S. Feng, R. Xu, Langmuir **15**, 8822–8825 (1999)
103. X. Shen, J. Zhang, B. Tian, J. Hazard. Mater. **192**, 651–657 (2011)
104. A. Zachariah, K.V. Baiju, S. Shukla, K.S. Deepa, J. James, K.G.K. Warrier, J. Phys. Chem. C **112**, 11345–11356 (2008)
105. A. Bojinova, R. Kralchevska, I. Poulios, C. Dushkin, Mater. Chem. Phys. **106**, 187–192 (2007)
106. Z. Liu, X. Zhang, S. Nishimoto, J. Ming, D.A. Tryk, T. Murakami, A. Fujishima, Langmuir **23**, 10916–10919 (2007)
107. R.G. Nair, S. Paul, S.K. Samdarshi, Sol. Energy Mater. Sol. Cells **95**, 1901–1907 (2011)
108. P.I. Gouma, M.J. Mills, J. Am. Ceram. Soc. **84**, 619–622 (2001)
109. Z. Jing, M. Li, Z. Feng, J. Chen, C. Li, J. Phys. Chem. B **110**, 927–935 (2006)
110. Y.C. Hsu, H.C. Lin, C.H. Chen, Y.T. Liao, C.M. Yang, J. Solid State Chem. **183**, 1917–1924 (2010)
111. M. Ni, M.K.H. Leung, D.Y.C. Leung, K. Sumathy, Renew. Sustain. Energy Rev. **11**, 401–425 (2007)

112. I.R. Oca09a, A. Beltram, J.J.D. Jaén, G. Adami, T. Montini, P. Fornasiero, Inorganica Chimica Acta (2015)
113. Q. Xu, Y. Ma, J. Zhang, X. Wang, Z. Feng, C. Li, J. Catal. **278**, 329–335 (2011)
114. Y.K. Kho, A. Iwase, W.Y. Teoh, L. M01dler, A. Kudo, R. Amal, J. Phys. Chem. C, **114**, 2821–2829 (2010)
115. F. Xu, W. Xiao, B. Cheng, J. Yu, Int. J. Hydrogen Energy **39**, 15394–15402 (2014)
116. O. Rosseler, M.V. Shankar, M.K.-L. Du, L. Schmidlin, N. Keller, V. Keller, J. Catal. **269**, 179–190 (2010)
117. G. Marcì, M. Addamo, V. Augugliaro, S. Coluccia, E. García-López, V. Loddo, G. Martra, L. Palmisano, M. Schiavello, J. Photochem. Photobiology A: Chem. **160**, 105–114 (2003)
118. L. Liu, H. Zhao, J.M. Andino, Y. Li, ACS Catal. **2**, 1817–1828 (2012)
119. H. Zhao, L. Liu, J.M. Andino, Y. Li, J. Mater. Chem. A **1**, 8209–8216 (2013)
120. S.N. Frank, A.J. Bard, J. Am. Chem. Soc. **99**, 303–304 (2002)
121. H. Xu, G. Li, G. Zhu, K. Zhu, S. Jin, Catal. Commun. **62**, 52–56 (2015)
122. Z. Luo, A. S. Poyraz, C. H. Kuo, R. Miao, Y. Meng, S. Y. Chen, T. Jiang, C. Wenos, S. L. Suib, Z. Luo, Chem. Mater. **27** (2014)
123. B. Zhao, Y. Jiao, F. Chen, H. Yang, J. Zhang, J. Mol. Catal. A: Chem. **348**, 114–119 (2011)
124. Y. Liao, W. Que, Q. Jia, Y. He, J. Zhang, P. Zhong, J. Mater. Chem. **22**, 7937–7944 (2012)
125. E. Grabowska, J. Reszczyńska, A. Zaleska, Water Res. **46**, 5453–5471 (2012)
126. Z. Ding, G. Lu, P. Greenfield, J. Phys. Chem. B **104**, 4815–4820 (2000)
127. B. Tian, C. Li, J. Zhang, Chem. Eng. J. **191**, 402–409 (2012)
128. R.I. Bickley, T. Gonzalez-Carreno, J.S. Lees, L. Palmisano, R.J.D. Tilley, J. Solid State Chem. (United States), **92:1**, 178–190 (1991)
129. N.A. Deskins, S. Kerisit, K.M. Rosso, M. Dupuis, J. Phys. Chem. C **111**, 9290–9298 (2007)
130. P. Deák, B. Aradi, T. Frauenheim, J. Phys. Chem. C **115**, 3443–3446 (2011)
131. D.O. Scanlon, C.W. Dunnill, J. Buckeridge, S.A. Shevlin, A.J. Logsdail, S.M. Woodley, C.R.A. Catlow, M.J. Powell, R.G. Palgrave, I.P. Parkin, Nat. Mater. **12**, 798–801 (2013)
132. A.K. Datye, G. Riegel, J.R. Bolton, M. Huang, M.R. Prairie, J. Solid State Chem. **115**, 236–239 (1995)
133. Z. Zhang, C.C. Wang, R. Zakaria, J.Y. Ying, J. Phys. Chem. B **102**, 10871–10878 (1998)
134. T. Ohno, K. Sarukawa, K. Tokieda, M. Matsumura, J. Catal. **203**, 82–86 (2001)
135. T. Kawahara, Y. Konishi, H. Tada, N. Tohge, J. Nishii, S. Ito, Angew. Chem. Int. Ed. Engl. **41**, 2811–2813 (2002)
136. G. Li, K.A. Gray, Chem. Phys. **339**, 173–187 (2007)
137. B. Sun, A.V. Vorontsov, P.G. Smirniotis, Langmuir **19**, 3151–3156 (2003)
138. S. Bo, P.G. Smirniotis, Catal. Today **88**, 49–59 (2003)
139. B. Liu, L. Peng, J. Alloy. Compd. **571**, 145–152 (2013)
140. G. Li, L. Chen, M.E. Graham, K.A. Gray, J. Mol. Catal. A: Chem. **275**, 30–35 (2007)
141. C.-Y. Wang, R. Pagel, J.K. Dohrmann, D.W. Bahnemann, C. R. Chim. **9**, 761–773 (2006)